URBAN DEVELOPMENT DIRECTORATE (UDD)

Ministry of Housing and Public Works

Government of the People's Republic of Bangladesh

REPORT ON WET SEASONAL DATA COLLECTION, ANALYSIS AND INTERPRETATION ALONG WITH SPATIAL DISTRIBUTION (GIS SHAPE FILE)

FOR THE PROJECT OF
HYDRO-GEOLOGICAL SURVEYS AND STUDIES

UNDER
PREPARATION OF DEVELOPMENT PLAN FOR MEHERPUR ZILLA

Package No.: 6 (Six)

June 2025

Submitted by

Center for Geoservices and Research
Flat# D1, House # 64/1,
Lake Circus, Kalabagan, Dhaka-1205

Contents

1 Disclaimer v

2 Acronyms vi

3 Introduction 1

4 Methodology: 2

4.1 Site Selection: 2

4.2 Drilling of Monitoring Wells: 5

4.3 Lithological Sampling and Logging: 5

4.4 Installation of Monitoring Wells 6

4.5 Development of Monitoring Wells 7

4.6 Water Level Measurement, Water Sampling and Slug Test 7

4.6.1 Water Level Measurement, Water Sampling in Monitoring Well 7

4.6.2 Water Sampling from Existing Wells 8

4.6.3 Slug Test 11

4.7 Electrical Resistivity Tomography 14

4.7.1 Methodology 15

4.7.2 Resistivity of Rocks 15

4.7.3 Resistivity Principles 15

4.7.4 Resistivity of Homogeneous Isotropic Medium 16

4.7.5 Basic Idea and Fundamentals of Resistivity Survey 20

4.7.6 ERT Data Acquisition 22

4.7.7 ERT Data Processing 23

5 Preliminary Results Based on Data Analysis 23

5.1 Groundwater Level 23

5.1.1 Groundwater Level in Deep Aquifers 24

5.1.2 Groundwater Level in Shallow and Intermediate Aquifer 28

5.2 Water Quality Data 28

6 Drought Analysis 29
6.1 Methodology: 30
6.2 Study Area 31
6.2.1 Data Collection 31
6.2.2 Data Processing 32
6.2.3 Gamma Distribution Fitting 33
6.2.4 SPI Calculation: 33
6.2.5 Mann-Kendall Trend Analysis 34
6.3 Results 35
6.3.1 Rainfall 35
6.3.2 Gamma Distribution: 37
6.3.3 SPI Timeseries Analysis 38
6.3.4 Drought Category: 42
6.3.5 Trend Analysis: 45
7 Discussion 47
8 References: 48
9 APPENDICES 49
9.1 APPENDIX: Table A-1: Location of Monitoring Well 50
9.2 APPENDIX: Table A-2: Location of VES 52

List of Figures

Figure 1: Cross Sectional View of Well Nest/Cluster 5
Figure 2: Drilling Procedure of Monitoring well in Mujibnagar Upazila. 6
Figure 3: Installation of Monitoring Well in Mujibnagar Upazila 7
Figure 4: Water Sampling and Field Test. 8
Figure 5: Water Sampling from Existing Well 9
Figure 6: Automatic data logger 11
Figure 7: Slug test in an existing well 12
Figure 8: Slug Test in a Monitoring Well 12

Figure 9: Estimation of aquifer properties from time-displacement data collected during an overdamped slug. 13
Figure 10 The parameters used in defining resistivity 16
Figure 11 Generalized form of the electrode configuration used in resistivity measurements 18
Figure 12 Wenner electrode configuration showing equal spacing 20
Figure 13 Wenner array ("a" is electrode spacing) and distribution of electric field underneath. (After Todd and Mays, 1980; Source: Wiwattanachang & Giao, 2011) 22
Figure 14: Measurement sequence for constructing a pseudo section. 23
Figure 15: Ground Water Level in MW-01 Vobanipur Primary School, Monakhali Union, Mujib Nagar, Meherpur 24
Figure 16: Ground Water Level in MW-02 Anandabas Dakkhin Para Govt Primary School, Bagoan Union, Mujib Nagar, Meherpur 25
Figure 17: Ground Water Level in MW-03 Ujalpur High School, Kutubpur Union, Meherpur Sadar, Meherpur 25
Figure 18: Ground Water Level in MW-04 Mominpur Govt Primary School, Pirojpur Union, Meherpur Sadar, Meherpur 26
Figure 19: Ground Water Level in MW-05 Bashbaria Govt Primary School, Gangni Paurashava, Gangni, Meherpur 26
Figure 20: Ground Water Level in MW-06 Baniapukur Govt Primary School, Shola Taka Union, Gangni, Meherpur 27
Figure 21: Ground Water Level in MW-07 Motmura Govt Primary School, Matmura Union, Gangni, Meherpur 27
Figure 22: Yearly Rainfall Distribution across 24 years in Meherpur District 36
Figure 23: Annual Rainfall and SPI values are shown for Meherpur District 39
Figure 24: SPI Timeseries Distribution from 1990 to 2025 40
Figure 25: Drought category percentage in Meherpur District from 1990 to 2024 43
Figure 26: Monthly Drought Categories Percentage in Meherpur District from 1990 to 2025 43
Figure 27: Seasonal average Drought duration months in Meherpur District 44
Figure 28: Seasonal Average SPI values in Meherpur District 45

List of Map

Map 1: Location map of the monitoring nests (Surface Geology Map) 3
Map 2: Location map of the monitoring nests (union-based map) 4
Map 3: Location of In-situ Test and Water Sampling in the Project Area 10
Map 4: Slug Test Location in Meherpur District (Source: BBS and CGR) 13
Map 5: Location Map of ERT (Data Source: BBS, CGR) 14

List of Table

Table 1: Number of Wells for Water Sampling and Field Test 29
Table 2: SPI and its relation to the impact on agriculture and water resources 30
Table 3: Monthly rainfall data aggregation to the corresponding SPI values 32
Table 4: Categories of drought scenarios based on SPI value range (McKee et al 1993) 34
Table 5: Monthly rainfall statistics, including the mean rainfall (in millimeters) and the skewness of the rainfall distribution for each month 36
Table 6: Results of Gamma Distribution Parameters for SPI Drought Analysis 37
Table 7: Mann Kendall trend statistics on three cropping seasons of the study area 46

1 Disclaimer

Every effort has been made to provide information that is current and accurate. Nevertheless, inadvertent errors in information may occur and every effort is made to ensure the data quality, the data is provided "as is".

Neither UDD, CGR nor any of its employees make any warranty, express or imply, including warranties of fitness for a particular purpose, or assume any legal liability or responsibility for the accuracy, completeness, or usefulness of any information provided (either isolated or in the aggregate), or represents that its use would not infringe privately owned rights. The designations employed and the presentation of the material in this publication do not imply the expression of any opinion whatsoever on the part of UDD, CGR, concerning the legal status of any country, territory, city or area or of its authorities, or concerning the delimitation of its frontiers or boundaries.

Managing Director

Center for Geoservices and Research

2 Acronyms

UDD	Urban Development Directorate
CGR	Center for Geoservices and Research
VES	Vertical Electrical Sounding
EC	Electrical Conductivity
TDS	Total Dissolved Solid
ASTM	American Society for Testing and Materials

3 Introduction

This report describes the collection of wet-season groundwater level data from seven (7) clustered, established monitoring wells in three upazilas of Meherpur District as part of the **hydrogeological surveys and studies** conducted under the Preparation of Development Plan for Meherpur Zilla project. Additionally, it includes details of a drought analysis for Meherpur Zilla, using the Standardized Precipitation Index (SPI) across four-time scales (SPI-1, -3, -6, and -12), based on CHIRPS rainfall data from 1990 to 2024. The results indicate increasing drought trends, particularly in SPI-6 and SPI-12 during the Kharif-2 and Rabi seasons, with rainfall variability significantly affecting groundwater recharge and agricultural productivity.

The establishment of these monitoring networks is the first step in a detailed hydrogeological investigation in the study area that will be carried out over the period of more than a year from now. A total of 21 monitoring wells have been drilled and installed at seven (07) locations. At each location, three (03) co-located wells (5 to 10 feet apart) have been installed at different depths. The deepest of each set is about 500 ± 100 feet deep, the intermediate one is about 300 feet deep, and the shallowest one is about 100 feet deep.

Groundwater levels in the study area will be monitored over an approximately one-year period, encompassing both dry and wet seasons, to evaluate seasonal variations in aquifer dynamics. As part of the wet-season dataset, groundwater level measurements were recorded from 22 March to 19 June 2025, covering the full pre-monsoon period and a portion of the monsoon season. This dataset is essential for characterizing hydrogeological conditions, assessing aquifer response to seasonal recharge, and establishing baseline fluctuations within the groundwater system.

As part of the ongoing groundwater monitoring program, the previous dry season report documented key physicochemical parameters, including electrical conductivity (EC), total dissolved solids (TDS), pH, and arsenic concentrations, derived from both production wells and newly established monitoring wells. During the in-situ field testing, the CGR team collected groundwater samples for laboratory-based ionic analysis. The target ions include Na^{+}, Ca^{2+}, Mg^{2+}, K^{+}, Fe, Mn, HCO_3^{-}, Cl^{-}, SO_4^{2-}, and NO_3^{-}, which are currently being analyzed at the Dhaka Laboratory. In addition, CGR performed slug tests to evaluate aquifer hydraulic properties. Grain size distribution analysis was also conducted in the laboratory to estimate the hydraulic conductivity (K) of various wells. The findings from these

investigations, along with **a full year of groundwater level monitoring data,** will be integrated into the forthcoming report titled "Report on Groundwater Scenario of the Whole Hydrological Year along with Identification of Potential Area of Groundwater Recharge and Drawing, and Surface water and Groundwater Interfacing Model including GIS Shapefile and Thematic Map."

Detailed methodology, locations, and collected data analysis are discussed in the subsequent sections.

4 Methodology:

In order to establish the monitoring network in the field, a field trip was carried out between 20th February and 22 March 2025. A team consisting of one geologist and one civil engineer worked together in the field for the entire period. The drilling team was employed to drill and install monitoring wells one by one. The detailed methodology for site selection, drilling, sampling, logging, and installation of the monitoring network is discussed in the subsequent sections.

4.1 Site Selection:

Monitoring well locations were selected first based on Geological, Geomorphological, and hydrogeological variability, and the location of existing data in the study area. Later, the locations were verified by physical observation and shifted a bit based on local access and available space for the investigation as well as the permission of the landowners. All the locations are verified finally, and permission is also obtained from the landowners. Locations of the monitoring wells are shown in Figure 1 and in Table A-1 in the Appendix.

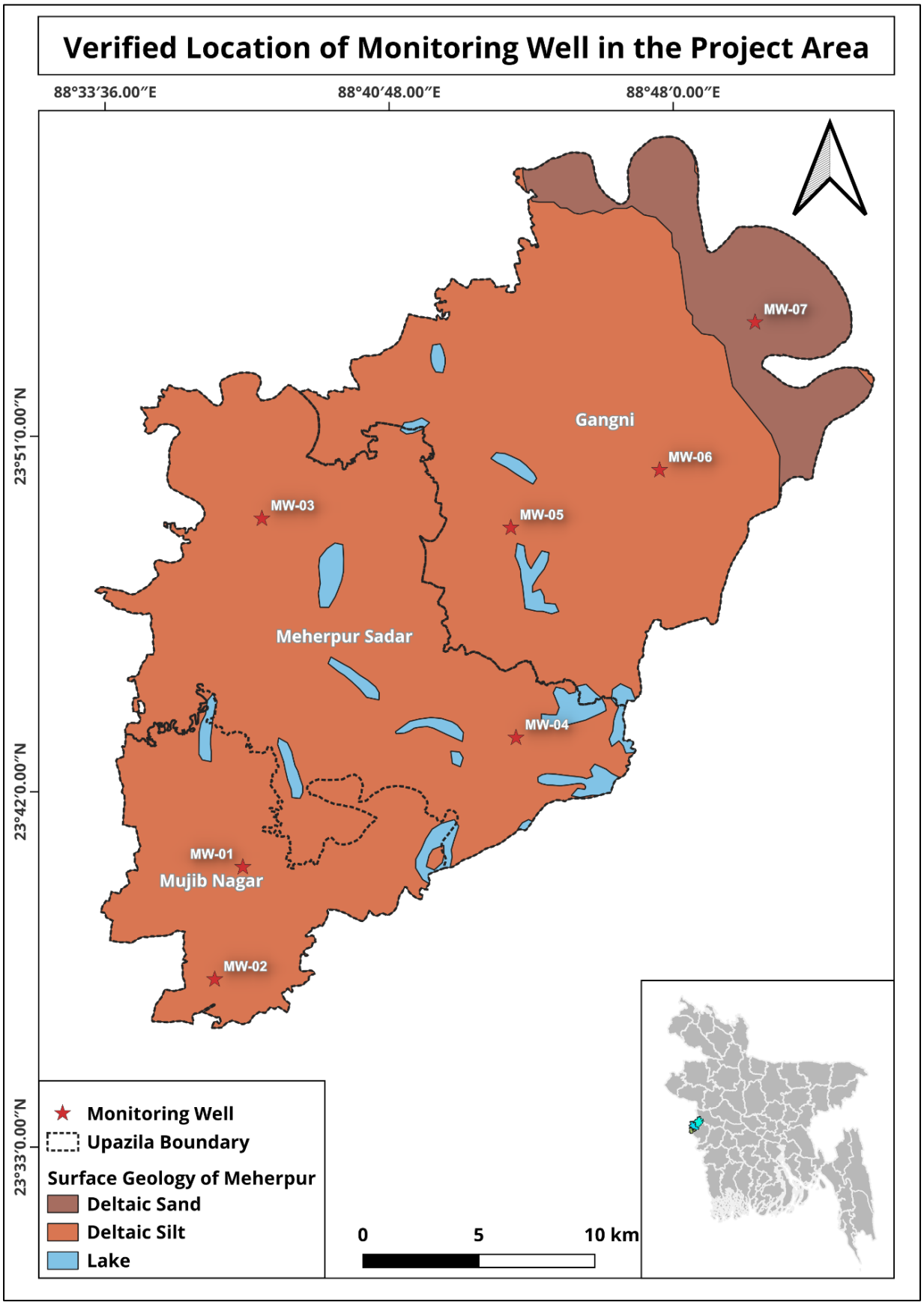

Map 1: Location map of the monitoring nests (Surface Geology Map)

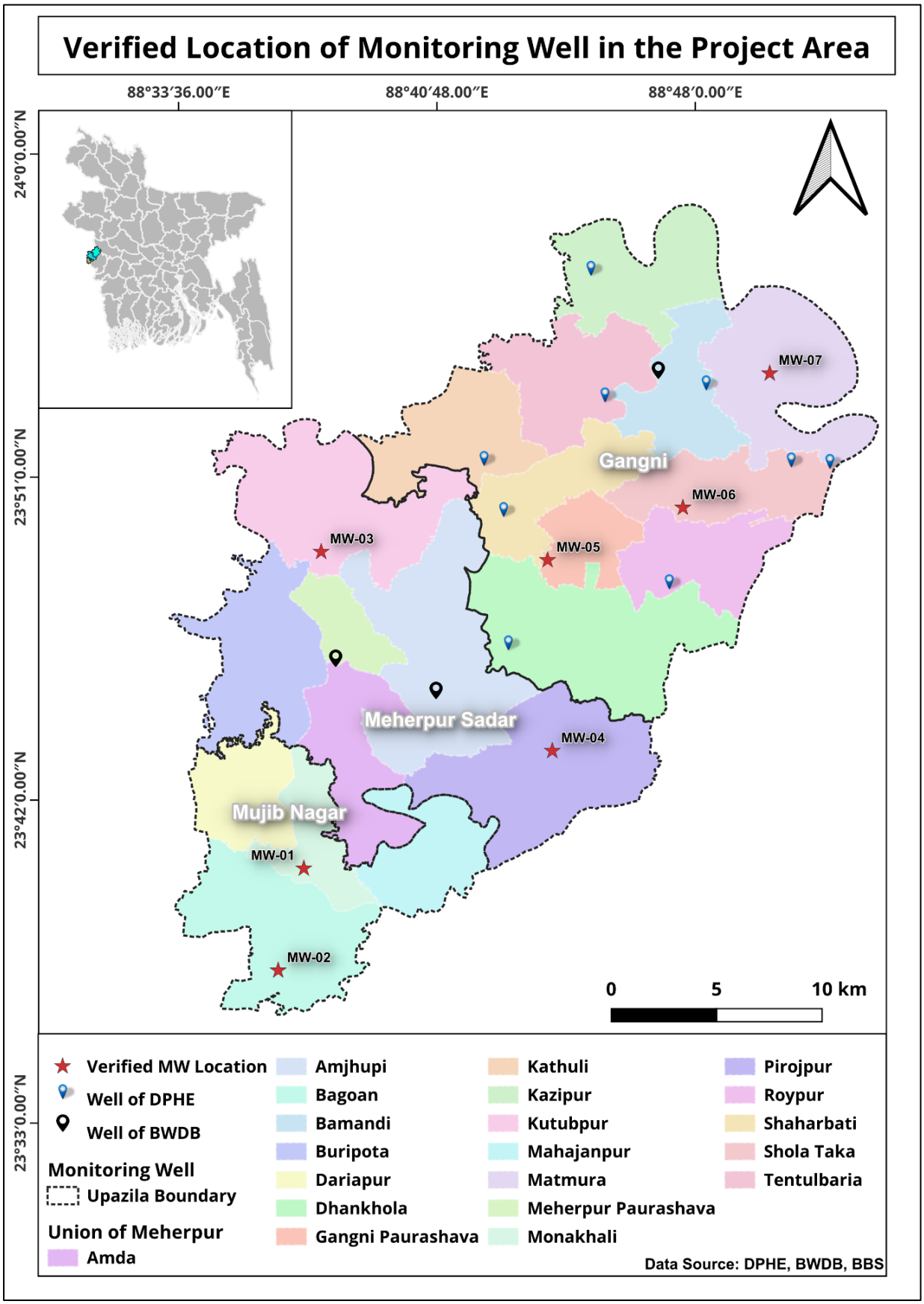

Map 2: Location map of the monitoring nests (union-based map)

4.2 Drilling of Monitoring Wells:

Since the groundwater quality in the study area varies in depth, monitoring wells at multiple depth intervals is essential. A total of 21 monitoring wells have been installed at seven (07) locations (one set of 3 wells, Map 1 and 2). At each location a cluster/nest[1] of three wells (one at around 500±120 feet depth, one at around 300±60 feet depth and the other at around 100 feet depth, each well will be within 5-10 ft from the other) have been installed as shown in Figure-2.

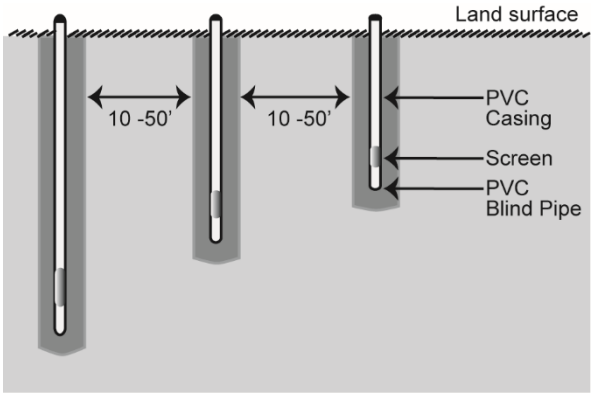

Figure 1: Cross Sectional View of Well Nest/Cluster

Reverse circulation conventional drilling method (Figure 3) was used for drilling the monitoring wells. In this method, drilling fluid enters the hole through the drill pipe and comes up to the surface with a mixture drill cutting through the annulus. Fluid was piped through the pipe using a high-speed mechanical pump. A mixture of water and cow dung was used as drilling fluids.

4.3 Lithological Sampling and Logging:

A well-site geologist was present at each site during drilling, responsible for logging the samples in a standard format and collecting samples at 10-foot intervals. He recorded the lithology on the log sheet provided by the consultancy firm, CGR, and preserved the samples for further laboratory testing, such as grain size analysis. The drill cuttings were collected in a bucket and stored in polyethylene bags for further laboratory analysis. The samples were visually analyzed by an onsite geologist, and a driller's log was prepared in the field.

---

[1] **Nest well:** A cluster of wells where tubes or pipes are constructed in separate (10-50 feet distance to each other), individual boreholes that are drilled and completed at different depths.

Figure 2: Drilling Procedure of Monitoring well in Mujibnagar Upazila.

4.4 Installation of Monitoring Wells

After the drilling was completed, a monitoring well was installed at every drill hole. The deep and intermediate monitoring wells have 20 feet screens at the bottom of the well but above 10 to 30 feet blind pipes. The shallower monitoring wells have 10 feet screen above 10 feet blind pipe. Both the well casing and screen consist of PVC materials (Figure-3). After installing the pipes, gravel packing was done around the well screen. The well annulus was back filled with clays collected during the drilling.

Figure 3: Installation of Monitoring Well in Mujibnagar Upazila

4.5 Development of Monitoring Wells

After installation, each monitoring well was developed using both manual pumping and an electrical compressor. Manual pumping was performed for several hours for the shallow wells, while the electrical compressor was used for up to tens of hours for the deep and intermediate wells until the electrical conductivity (EC) of the well water stabilized. A local hand pump was used for manual pumping during well development.

4.6 Water Level Measurement, Water Sampling and Slug Test

The slug testing and water sampling campaign was conducted in two distinct phases. **Phase 1** focused on existing production wells and was carried out from 1 January 2025 to 8 January 2025. During this phase, slug tests were performed at 60 existing production wells, and water sampling along with in-situ water quality testing was conducted at 35 of these wells. **Phase 2** targeted the newly installed monitoring wells and took place from 18 May 2025 to 21 May 2025. In this phase, all field activities were conducted in the 21 newly established monitoring wells, providing comprehensive data for further hydrogeological analysis.

The description of water level measurement, water sampling and slug is given below:

4.6.1 Water Level Measurement, Water Sampling in Monitoring Well

After the successful development of the monitoring wells, groundwater levels at the monitoring wells were measured using an electronic groundwater level meter. Afterwards,

the wells were pumped, and water samples were collected for laboratory analysis. During water sampling, a number of onsite geochemical parameters were also measured in the field using field test kits. These parameters include pH, electrical conductivity (EC), total dissolved solids (TDS), and arsenic (Figures 4).

Water levels will be measured automatically at hourly intervals in the deep wells using automatic data loggers for a period of one year. In shallow and intermediate wells, water levels will be measured biweekly using a water level meter for the same period.

Figure 4: Water Sampling and Field Test.

4.6.2 Water Sampling from Existing Wells

A total of 35 existing wells were sampled in 3 Upazilas. Before sampling each well was purged for 5-10 minutes. Samples were collected in 100 ml plastic bottles. Two samples were collected from each well; one was acidified by Nitric acid (HNO_3), and the other was non-acidified. Both samples were filtered before filling the sampling bottle. Each sample was given a sample ID, and the sample bottle was labeled with ID. In addition to sample collection, several onsite geochemical parameters were measured in the field using field test kits. These parameters include pH, Electrical conductivity (EC), TDS, and Arsenic (Figure 5). Details of the sample locations and field parameters are given in Table A-3 in Appendix.

Figure 5: Water Sampling from Existing Well

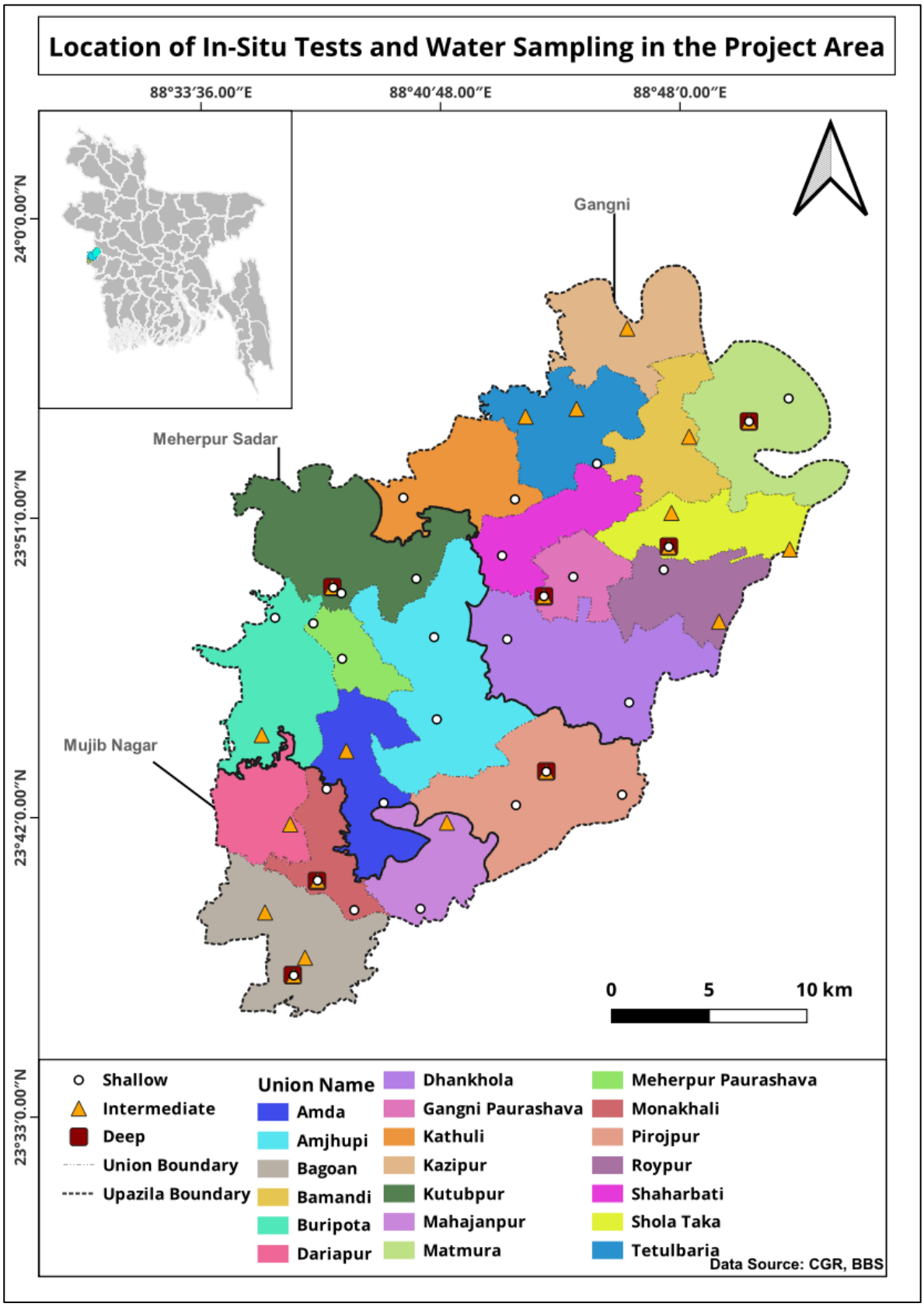

Map 3: Location of In-situ Test and Water Sampling in the Project Area

4.6.3 Slug Test

Slug tests were conducted at a total of 81 locations across the study area, including 60 existing hand tube wells and 21 newly installed monitoring wells. (Map: 4). Since pump tests are very expensive, they are usually carried out at only a few locations, providing very sparse data on the aquifer properties. A cheap alternative of pump test is slug test. For high density coverage of hydraulic conductivity data slug test will be performed in a large number of wells throughout the study area. Slug test is a field method where a slug (usually a rod) is inserted in a well below the water table, which causes an instantaneous rise of water level in the well. Dissipation of the water level in the well is then recorded, usually by an automatic water level logger (Figure 6). The temporal rate of this water level declines provides information on the hydraulic conductivity and specific yield/storage of the aquifer surrounding the well. This is a quick but accurate method of estimating hydraulic conductivity in any small diameter tube wells.

Figure 6: Automatic data logger

A slug test is a controlled field experiment, performed by groundwater hydrologists to estimate the hydraulic properties of aquifers and aquitards, in which the water level in a control well is caused to change suddenly (rise or fall) and the subsequent water-level response (displacement or change from static) is measured through time in the control well and one or more surrounding observation wells (Figure 7 & 8).

Figure 7: Slug test in an existing well

Slug tests are frequently designated as rising-head or falling-head tests to describe water-level recovery in the control well following test initiation. Other terms sometimes used instead of slug test include baildown test, slug-in test and slug-out test. The goal of a slug test, as in any aquifer test, is to estimate hydraulic properties of an aquifer system such as hydraulic conductivity.

Figure 8: Slug Test in a Monitoring Well

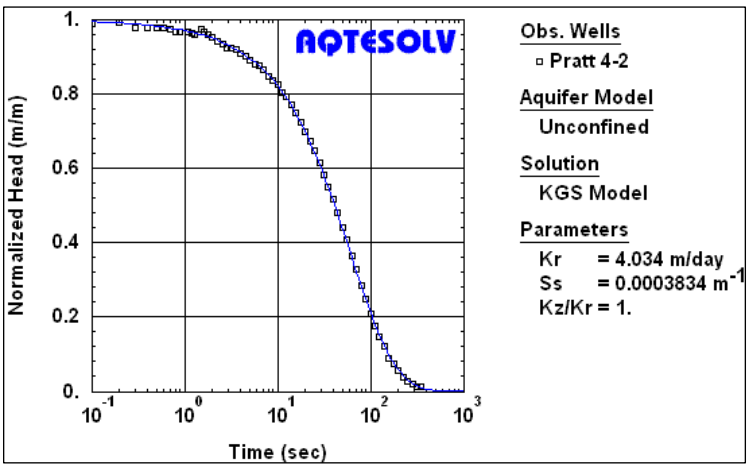

Figure 9: Estimation of aquifer properties from time-displacement data collected during an overdamped slug.

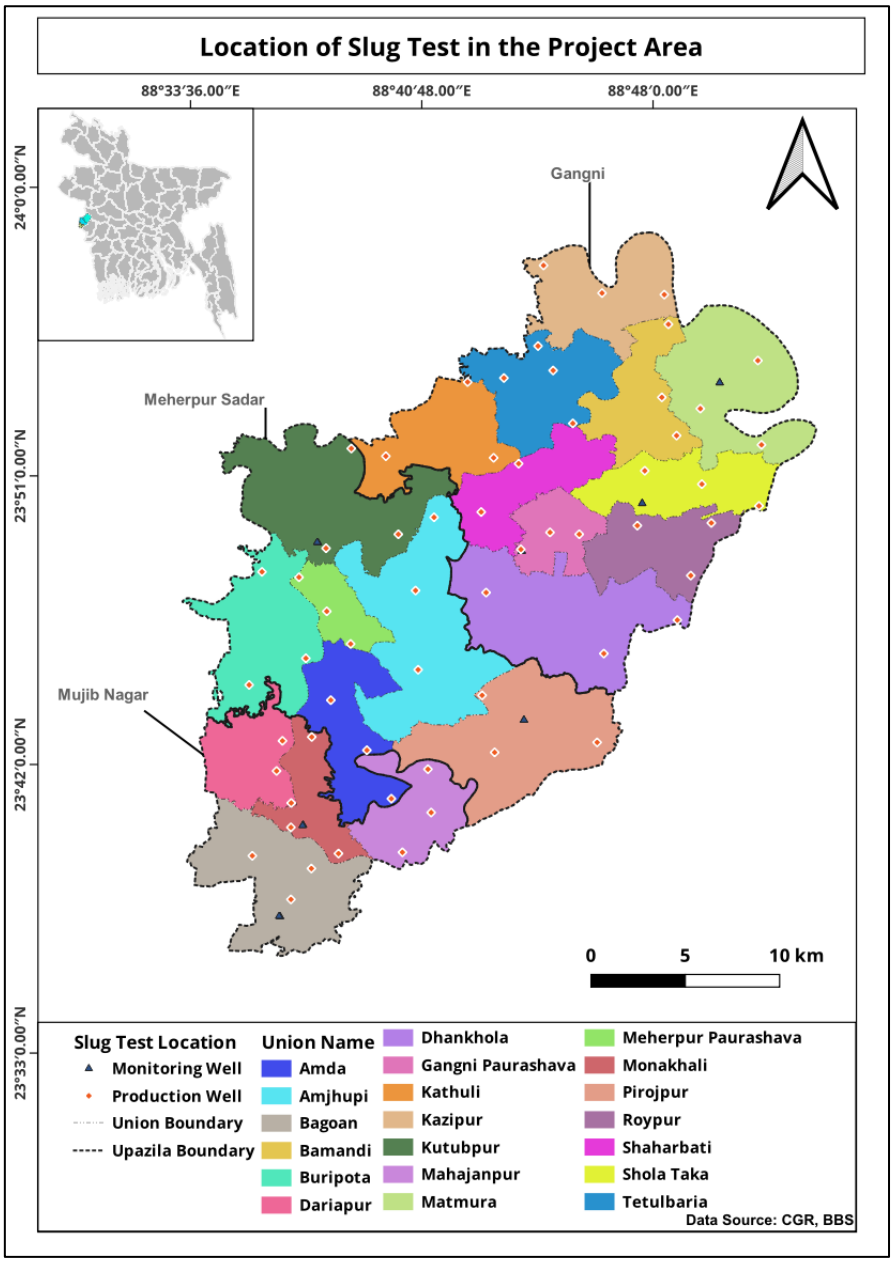

Map 4: Slug Test Location in Meherpur District (Source: BBS and CGR)

4.7 Electrical Resistivity Tomography

Boreholes provide direct information about the subsurface. However, drilling boreholes is expensive and their density in an area is usually low resulting in a spare point data about the subsurface geology. Interpolation of these sparse data for mapping subsurface geology/aquifers can be erroneous since usually there are data gaps over a large area between each borehole. Geophysical methods can be very useful in minimizing the data gap. In this study, Electrical Resistivity Tomography (ERT) surveys are planned to be conducted at 15 selected sites across three Upazilas (as shown in Map 5). The data acquisition will commence following the end of the rainy season to ensure optimal subsurface measurement conditions.

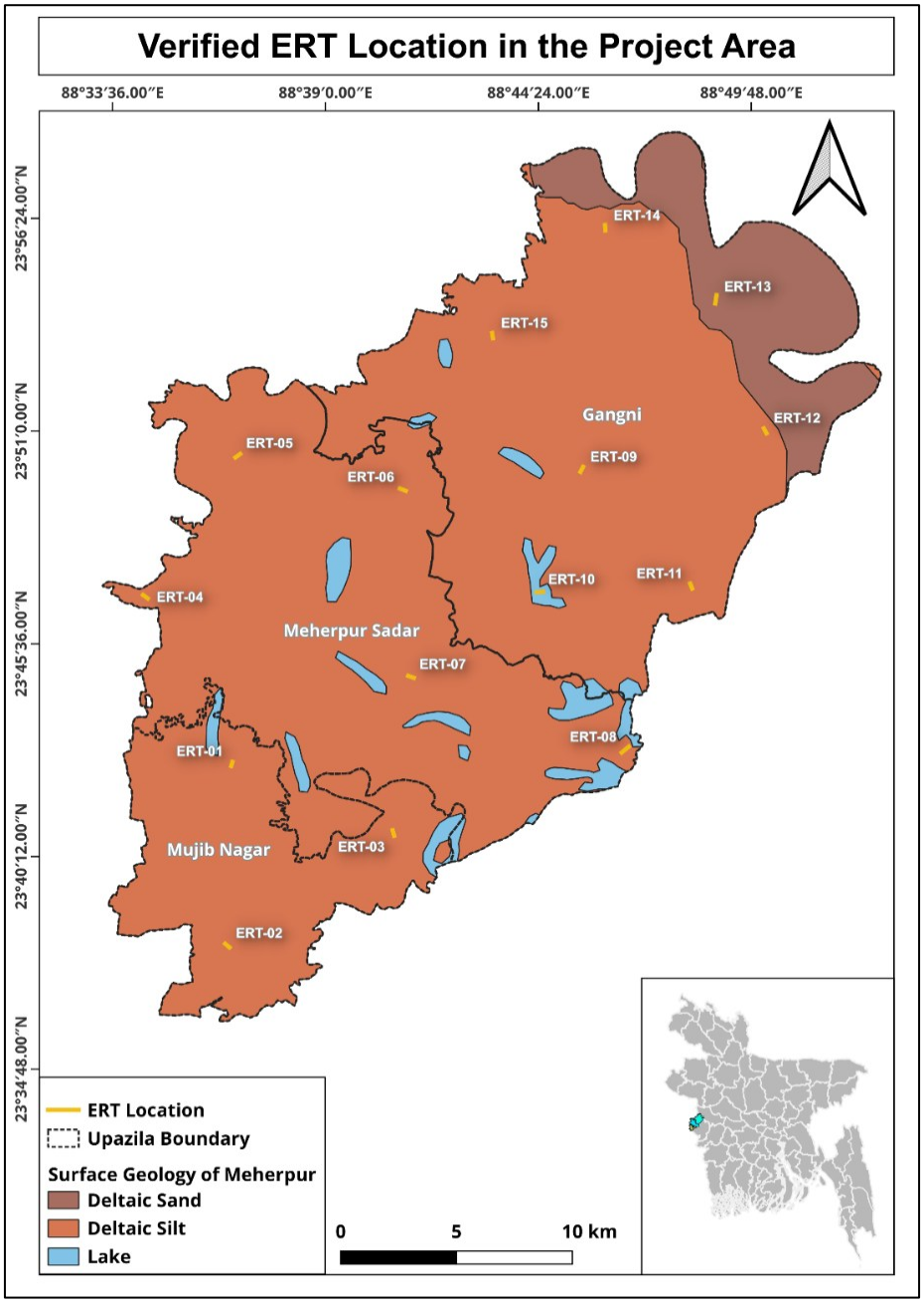

Map 5: Location Map of ERT (Data Source: BBS, CGR)

4.7.1 Methodology

Geo-electrical resistivity surveys have long been used for geo-engineering studies, and the method is found to be very successful. Geophysical methods are now widely used in solving complicated geological, hydrological, and environmental problems. Among all the geophysical methods, electrical and electromagnetic techniques are the most popular in groundwater exploration, geotechnical investigations, disaster science due to the close inter-relationship among electrical conductivity, hydrogeological properties of the aquifer such as porosity, clay content, mineralization of the groundwater, degree of water saturation, and lithology. Several case histories conducted in different parts of the world proved that the conventional direct current (DC) resistivity method is one of the most effective tools to decipher the underlying soil conditions in complicated geological settings.

4.7.2 Resistivity of Rocks

The resistivity of rocks varies considerably with lithology. The resistivity of rocks varies considerably with lithology. Sediments comprising aquifers are sands of various grain sizes. The electrical conductivity of these sediments depends on the salt concentration of the pore space water they contain. Clay and silt, rich in water-soluble minerals, have low resistivity even when their water content is low. The conductivity of sand and gravel is exclusively the consequence of their pore space water content, as they are composed of electrically non-conducting minerals. Consequently, sand and gravel show very high specific resistivity above groundwater level, and lower values below it. Resistivity is usually the most important property in determining the flow of electric current.

4.7.3 Resistivity Principles

In the resistivity method, artificially generated electric currents are introduced into the ground, and the resulting potential differences are measured at the surface. Generally, actual resistivity values are determined from apparent resistivity, which are computed from the measurements of current and potential differences between two pairs of electrodes placed on the ground surface. Two main types of procedures related to the resistivity survey are: vertical electrical sounding (VES) and constant separation traversing (CST). In groundwater exploration, vertical electrical sounding is widely used to identify the aquifer position, their lateral extent, variations in thickness, and water quality.

The resistivity of a material is defined as the resistance in ohms between the opposite faces of a unit cube of the material. For a conducting cylinder of resistance ΔR with a cross-sectional area ΔA and a length ΔL (Fig. 1), the resistivity of the cylinder can be expressed as:

$$\rho = \Delta R. \Delta A / \Delta L$$

The SI unit of resistivity is ohm-meter (Ω-m). The reciprocal of resistivity is termed as the conductivity and the SI unit of conductivity is ohm per meter or Siemens. The Ohm's law, which states that temperature remaining constant, the potential difference 'V' across a current bearing conductor is given by the product of the current 'I' and the resistance 'R' of the conductor.

$$V=IR \qquad (1)$$

Let the conductor be a plate of thickness 'L' and area of cross-section 'A', then

$$R= \rho L/A \qquad (2)$$

Where ρ is the resistivity of the plate

Putting equation (2) in equation (1) we get,

$$V = I\rho L/A,$$

$$\text{Or, } V= j\rho L \quad [j =I/A= \text{current density}] \qquad (3)$$

If 'L' is very small, the potential difference 'V' will also be small Δv, then the ratio $-\Delta v/\Delta l$ is given by the potential gradient E

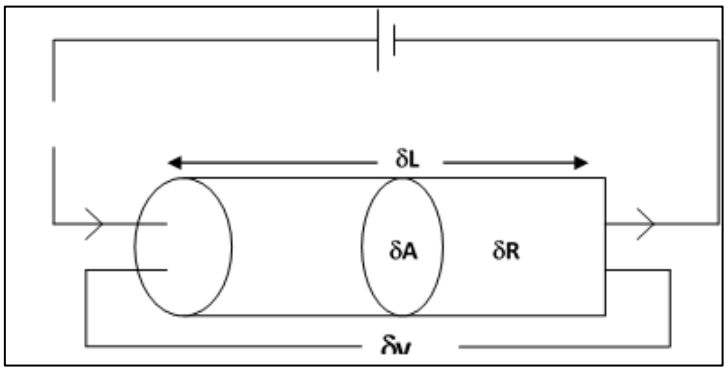

Figure 10 The parameters used in defining resistivity

Therefore, $-\Delta v/\Delta l = E= j\rho$ or

$$j = E/\rho = \sigma E \qquad (4)$$

Where, σ is the conductivity of the plate.

4.7.4 Resistivity of Homogeneous Isotropic Medium

The simplest approach to the theoretical study of earth resistivity measurements is to consider first the case of a completely homogeneous isotropic path. An equation giving the potential about a single point source of current on the spherical surface can be developed from ohm's

law. In homogeneous isotropic ground where there is a point source of current below the ground surface, the current radiates equally in all directions. Hence the equipotential surfaces are spherical with center at source point. For two such equipotential surfaces very near to each other the potential difference would be v_1-v_2= Δv between them.

If the radial distance between them is Δr, then potential gradient E at any point between them is

$$-\Delta v/\Delta r = E$$

The current density 'j' at any point on the equipotential surfaces would be

$$j = I/4\pi r^2$$

By ohms law,

$$J = I/4\pi r^2 = \sigma E = -\sigma\, \Delta v/\Delta r$$

$$\text{Or, } \Delta v/\Delta r = -\, 1/\sigma.\ I/4\pi r^2$$

$$\therefore \Delta v = -\, 1/\sigma.\ I/4\pi r^2.\Delta r \qquad (5)$$

Now, integrating the equation (5) we get,

$$V = 1/\sigma.\ I/4\pi r + C$$

$$V = \rho I/4\pi r \qquad (6)$$

$$\text{When } \ r = \infty \rightarrow C = 0.$$

If the point source of current is at the ground surface, then the current will flow hemispherically, then equation (6) can be expressed as

$$V = \rho I/2\pi r \qquad (7)$$

Potential functions are scalars and so, may be added arithmetically. If there are several sources of current rather than the single source assumed so far, the total potential at an observation point may be calculated by adding the potential contributions from each source independently. Thus, for n current sources distributed in a uniform medium, the potentials at an observation point, M will be-

$$V_M = \rho/2\pi\ [I_1/a_1 + I_2/a_2 + \text{----------} + I_n/a_n] \qquad (8)$$

Where, I_n is the current from the n^{th} in a series of current electrodes and a_n is the distance from the n^{th} source to the point at which the potential is being observed.

Equation (8) is of practical importance in the determination of earth resistivities. The physical quantities measured in a field determination of resistivity are the current, I, flowing between two current electrodes; the difference in potential ΔV, between two measuring points and the distance between the various electrodes.

When there are two current electrodes (A&B) on ground surface and the distance between two current electrodes is finite (Figure 12), the potential at any nearby surface point will be affected by both current electrodes.

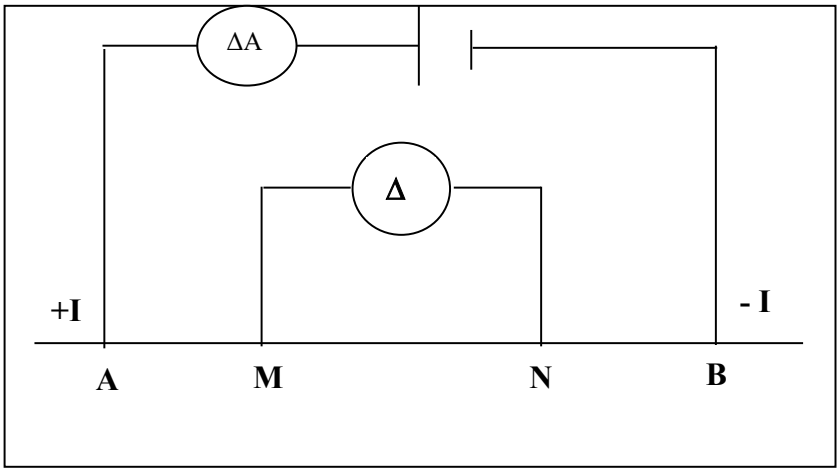

Figure 11 Generalized form of the electrode configuration used in resistivity measurements

The potential V_m at an internal potential electrode M_c is the sum of the potential contributions V_A and V_B from the current source at A and the sink at B.

$$V_M = V_A - V_B$$

From the equation (7) we get,

$$V_M = \rho I/2\pi\ (1/AM - 1/BM) \qquad (9)$$

Similarly,

$$V_N = \rho I/2\pi\ (1/AN - 1/BN) \qquad (10)$$

Absolute potentials are difficult to monitor so the potential difference ΔV between two electrodes 'M' and 'N' is measured:

$$\Delta V = V_M - V_N = \rho I/2\pi\ \{(1/AM - 1/BM) - (1/AN - 1/BN)\}$$

$$\text{Thus } \rho = 2\pi\ \Delta V/I\ \{(1/AM - 1/BM) - (1/AN - 1/BN)\} \qquad (11)$$

The equation (11) is applied for the ordinary four terminal arrays in measuring the earth resistivity in the field. Where the ground is uniform, the resistivity calculated from equation (11) should be constant and independent of both electrode spacing and surface location. When subsurface in homogeneities exist, the resistivity will vary with the relative positions of the electrodes. Any computed value is then known as the apparent resistivity (ρ_a) and will be a function of the form of the in homogeneity. Equation (11) is basic equation for calculating the apparent resistivity for any electrode configuration.

The arrangement of current and potential electrodes on or in the ground for the purpose of making an electrical survey is called electrode configuration. The current electrodes are generally placed on the outside of the potential electrodes.

Based on the position of current or potential electrodes and variation in distance between them, a variety of electrode configurations are possible of which some are mentioned below:

I. Wenner configuration

II. Schlumberger configuration

III. Dipole-dipole configuration

The choice of array and distance between the electrodes is very important for obtaining the best possible information of the subsurface geology of a given area. For ERT, Wenner configuration is preferred.

The Wenner configuration, in which potential difference is measured, is one of the simpler and most commonly used electrode arrays for determining resistivity. This is a symmetrical configuration consisting of four electrodes, the outer two electrodes are current electrodes and the inner two electrodes are potential electrodes. The distance between any two adjacent electrodes is called the array spacing and is equal and usually denoted by 'a' along a straight line (Figure 13).

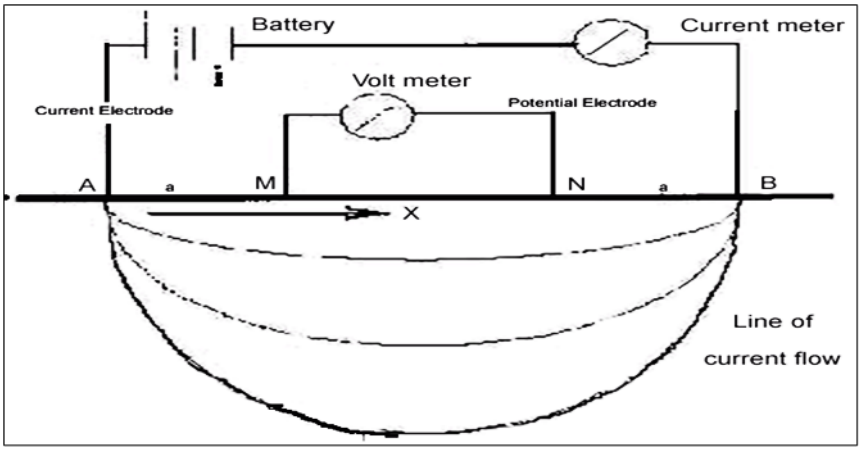

Figure 12 Wenner electrode configuration showing equal spacing

In spite of the simple geometry, this arrangement is quite often inconvenient for fieldwork. This arrangement has some disadvantages from a theoreticalpoint of view. For depth exploration using the Wenner configuration, the electrodes are expanded about a fixed center, increasing the spacing 'a' insteps. In case of lateral exploration of mapping, the spacing remains constant and all four electrodes are moved along the line, then along another line and so on.

The apparent resistivity with the Wenner array is given by-

$$\rho a = 2\pi a \, . \, \Delta V/I$$

Where,

ΔV = Potential difference in volts between V1 and V2;

I = Current in ampere;

a = Array spacing;

ρa = Apparent resistivity;

The geometric factor of Wenner configuration is $2\pi a$;

the resistivity of subsurface rock depends on this factor.

4.7.5 Basic Idea and Fundamentals of Resistivity Survey

Geo-electrical resistivity survey has long been used for ground water survey and the method is found to be very successful. As a preliminary step for the development of ground water, geo electrical resistivity survey proved to be very effective- (Bugg & Lloyed, 1976; Serres, 1969; Urish & Frohlich, 1990; Woobaidullah et al, 1996). In resistivity method, artificially

generated electric currents are introduced into the ground and the resulting potential differences are measured at the surface. Generally actual resistivities are determined from apparent resistivities, which are computed from the measurements of current and potential differences between two pairs of electrodes placed in the ground surface. The procedure involves measuring a potential difference between two potential electrodes (M & N) resulting from an applied current through two other current electrodes (A & B) outside but in line with the potential electrodes. Thus, the measured current and potential differences yield an apparent resistivity over an unspecified depth. If the spacing between the electrodes is increased penetration of the electric field also increases and a different apparent resistivity is obtained. Two main type resistivity surveys are: Vertical Electrical Sounding and Constant Separation Traversing/ Profiling (CST).

Vertical Electrical Sounding sees the current and potential electrodes at the same relative spacing and the whole spread is progressively expanded about a fixed central point. Consequently, readings are taken as the current reaches progressively greater depths. In this case Schlumberger configuration is favored. Constant Separation Traversing is used to determine the lateral variations of resistivity. The current and potential electrodes are maintained at a fixed separation and progressively moved along a profile. In this case Wenner configuration is favored.

Electric Resistivity Tomography (ERT) is a robust and well-consolidated method for near-surface geophysics, with a wide spectrum of applications in the geological, engineering and environmental sciences. Technological advances (e.g., multi-channel arrays, innovative sensors) and novel tomographic algorithms for data inversion have rapidly transformed ERT into one of the most employed geophysical methods. In essence, the survey procedures are similar to CST, but with each increment in electrode spacing, the survey direction is reversed.

As for data processing, an inversion model is conducted. The least-squares method is used to calculate certain physical characteristics of the subsurface, the “model parameters”, from the apparent resistivity measurements. The “model parameters” are set by the way we slice and dice the subsurface into different regions. The method most commonly used in 2-D interpretation is a purely cell-based model where the subsurface is subdivided into rectangular cells. The positions of the cells are fixed and only the resistivity values of cells are allowed to vary during the inversion process. The model parameter is the resistivity of each cell.

4.7.6 ERT Data Acquisition

To define the subsurface resistivity condition Wenner configuration (WN) has been used. Four equally spaced electrodes are used in WN where two outer electrodes (A & B) acted as current electrodes (source) and two inner electrodes (M & N) acted as potential electrodes (Figure 14). The array spacing expands about the array midpoint while maintaining an equivalent spacing between each electrode (Keller, 1996). The resistivity measured by this configuration can be determined from the readings of current intensity (I) and the potential difference between M and N (ΔV) values as follows:

$$\rho A = k\frac{\Delta V}{I}$$

Where ρA is the apparent resistivity, k is the geometric factor as defined by the following expression:

$$k = \frac{2\pi}{\left(\frac{1}{AM} - \frac{1}{BN} - \frac{1}{AN} + \frac{1}{BN}\right)}$$

The Wenner array employed in this study is one of the most commonly used arrangements, in the field.

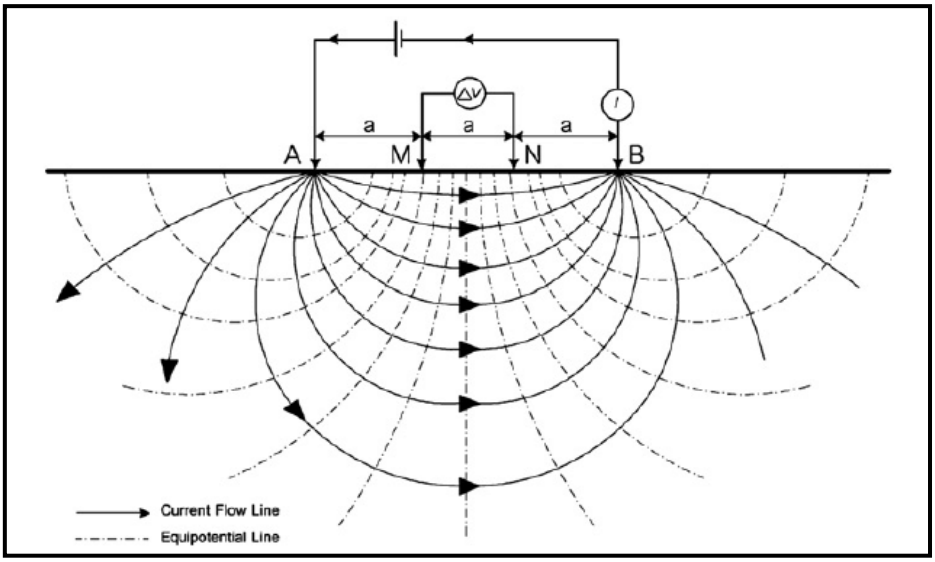

Figure 13 Wenner array ("a" is electrode spacing) and distribution of electric field underneath. (After Todd and Mays, 1980; Source: Wiwattanachang & Giao, 2011)

A spacing "a" separates the four electrodes equally. Wenner array's geometric coefficient is equal to 2a (Wiwattanachang & Giao, 2011). As a result, the apparent resistivity is determined as follows:

$$\rho A = 2\pi a \frac{\Delta V}{I}$$

Wenner configuration with a spread length of 90 m maximum is planned to execute where the electrode spacing was 3, 6, 9, 12 and 15 m respectively in all 20 sites in the investigated area.

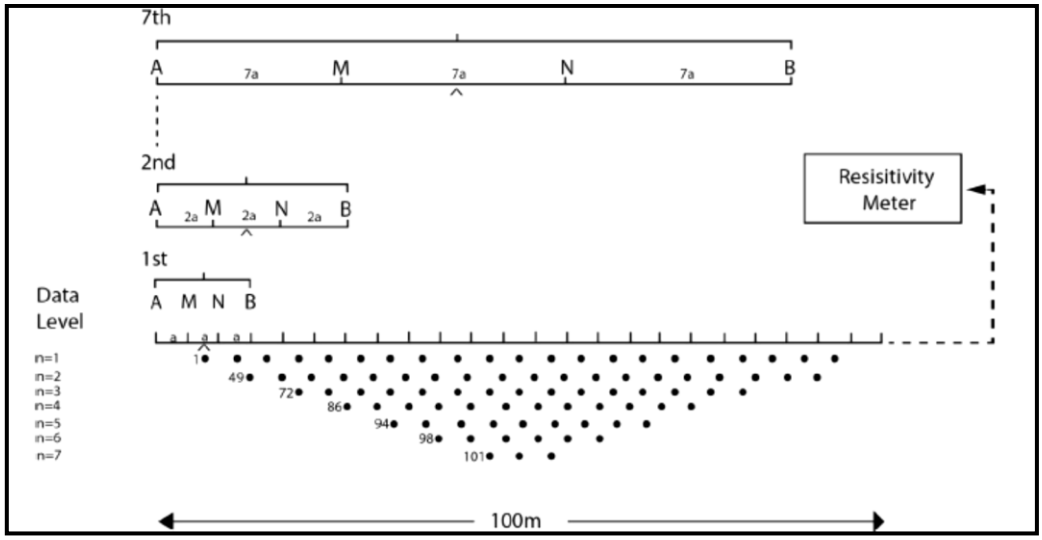

Figure 14: Measurement sequence for constructing a pseudo section.

4.7.7 ERT Data Processing

The measured data were converted into a suitable (.dat) format and therefore inverted using the smoothness-constrained least-squares inversion method in the Res2Dinv software (Loke and Barker, 1996; Sasaki 1992; deGroot-Hedlin and Constable 1990). The smoothness-constrained least-squares method is based on the following equation:

$$(\mathbf{J}^{\mathrm{T}}\mathbf{J} + u\mathbf{F})\,\mathbf{d} = \mathbf{J}^{\mathrm{T}}\mathbf{g}$$

Where, F = fxfxT + fzfzT; fx = horizontal flatness filter; fz = vertical flatness filter.

J = matrix of partial derivatives; u = damping factor; d = model perturbation vector; g = discrepancy vector.

5 Preliminary Results Based on Data Analysis

5.1 Groundwater Level

Bangladesh experiences three distinct climatic seasons: the pre-monsoon hot season (March–May), the monsoon or rainy season (June–October), and the cool dry winter season (November–February). Groundwater level fluctuation data has been collected over an approximately three-month duration spanning the transition from the pre-monsoon to the

monsoon season. To monitor groundwater dynamics, an automated data logger was installed in a deep monitoring well to record water level variations at specified intervals. Monitoring Well MW-06 was configured to log water levels on a daily basis, while all other deep monitoring wells recorded data on a weekly schedule. In parallel, manual water level measurements were conducted monthly in both shallow and intermediate-depth monitoring wells to complement the automated dataset.

5.1.1 Groundwater Level in Deep Aquifers

In the three aquifer zones, all aquifers exhibit minimal variation in groundwater levels over time. Between 22 March 2025 and 19 June 2025, the groundwater level in all deep wells fluctuated by more than 0.5 meters.

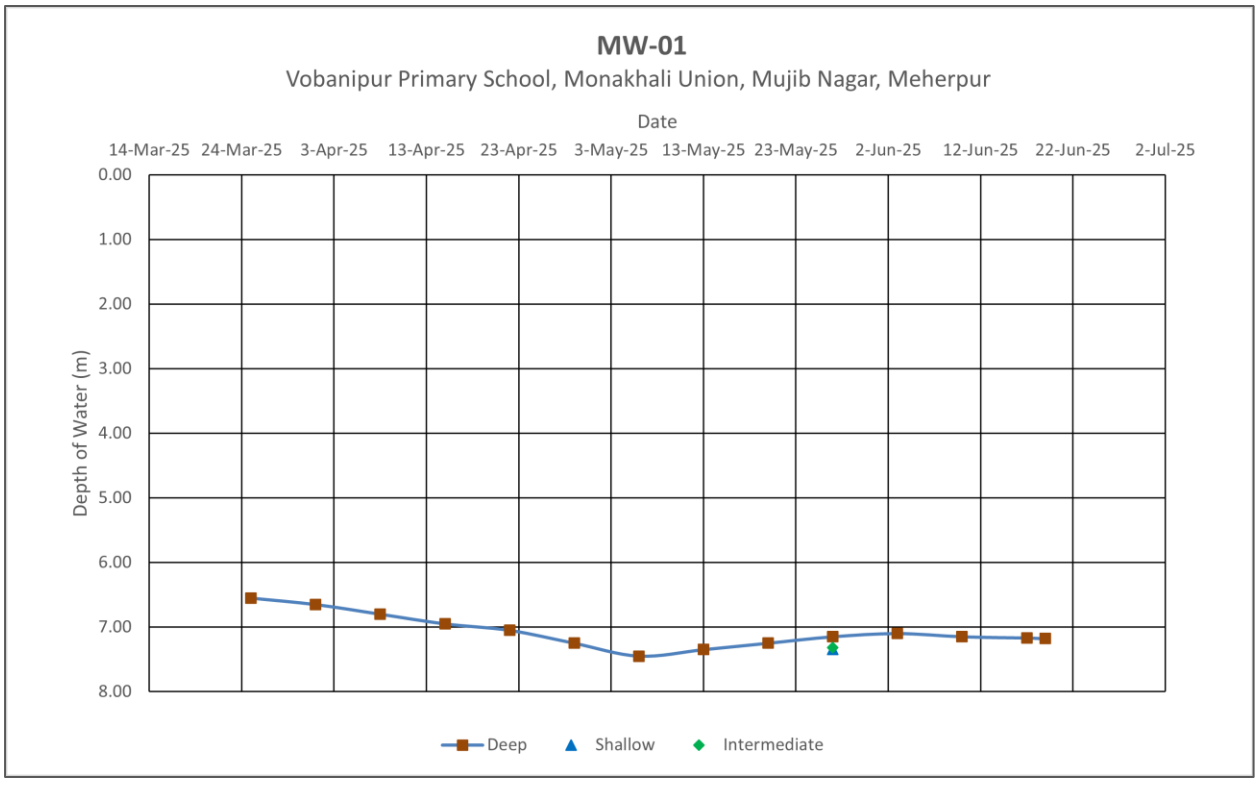

Figure 15: Ground Water Level in MW-01 Vobanipur Primary School, Monakhali Union, Mujib Nagar, Meherpur

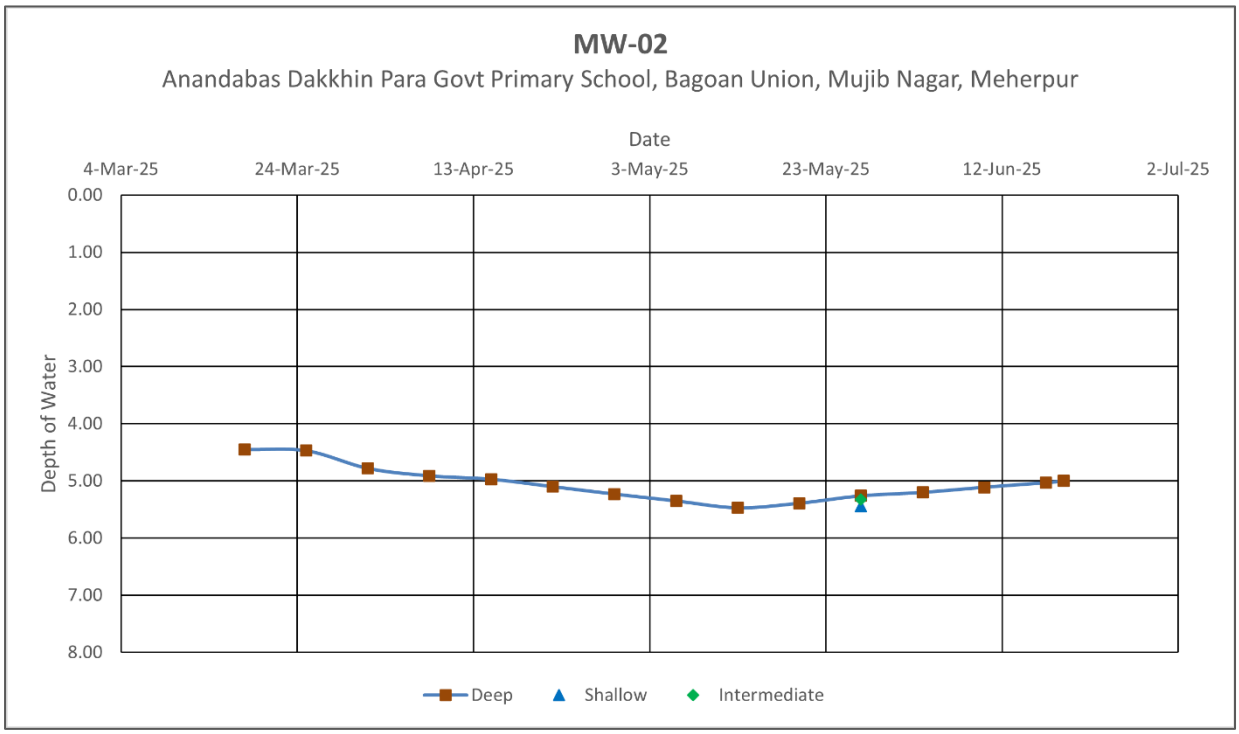

Figure 16: Ground Water Level in MW-02 Anandabas Dakkhin Para Govt Primary School, Bagoan Union, Mujib Nagar, Meherpur

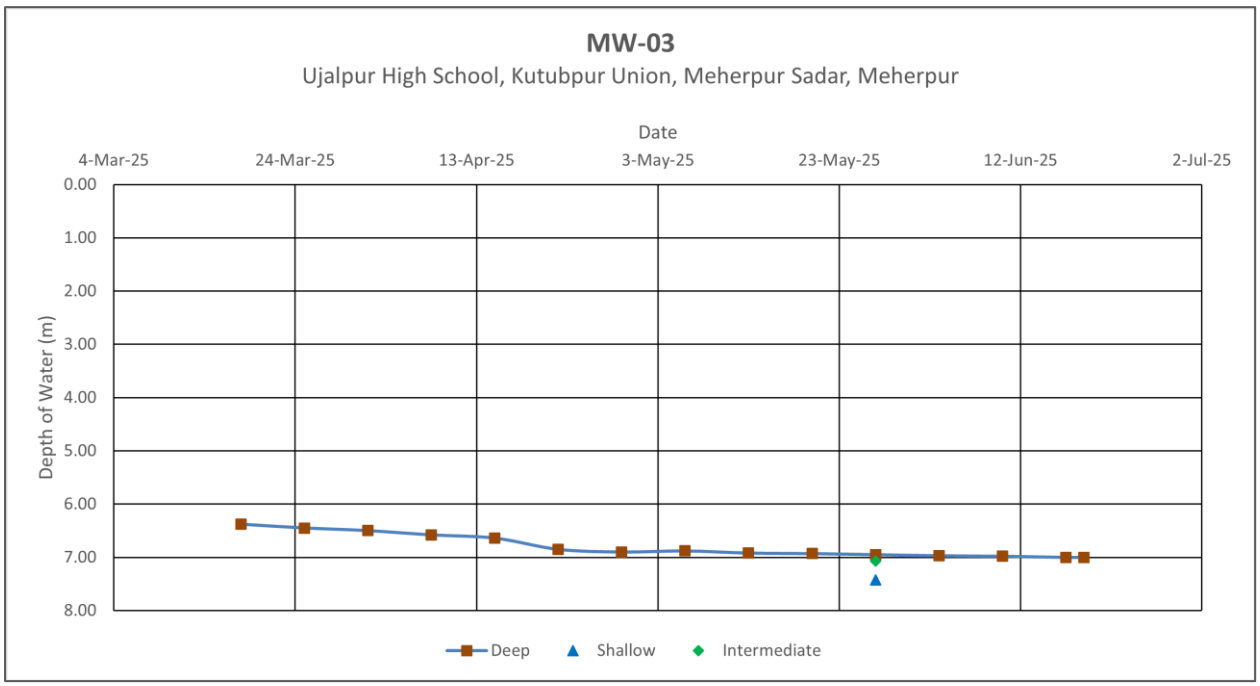

Figure 17: Ground Water Level in MW-03 Ujalpur High School, Kutubpur Union, Meherpur Sadar, Meherpur

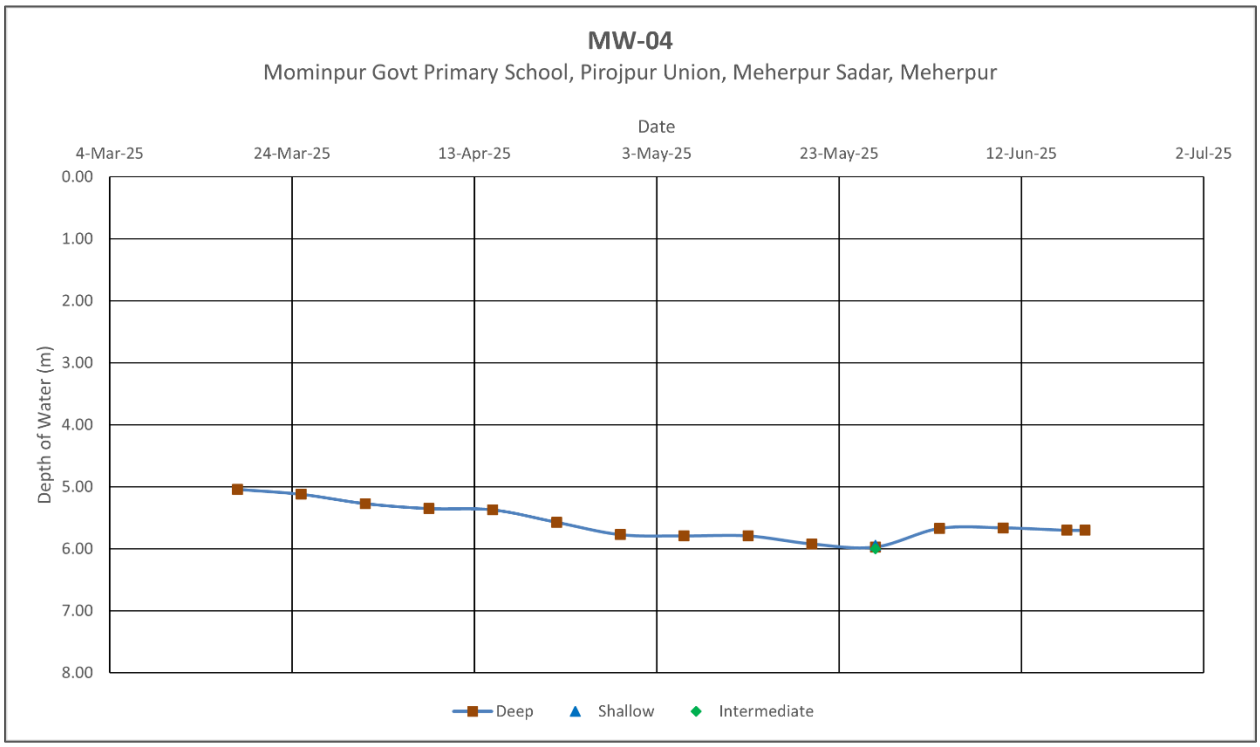

Figure 18: Ground Water Level in MW-04 Mominpur Govt Primary School, Pirojpur Union, Meherpur Sadar, Meherpur

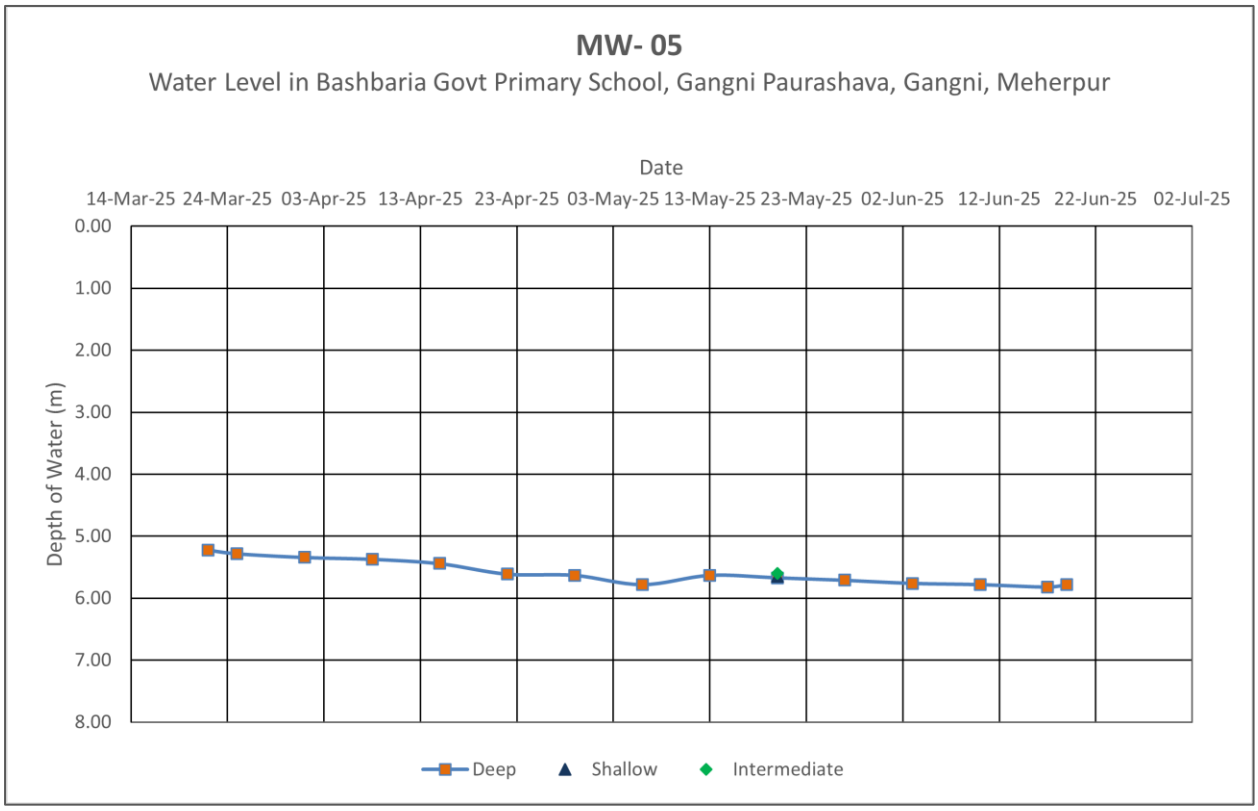

Figure 19: Ground Water Level in MW-05 Bashbaria Govt Primary School, Gangni Paurashava, Gangni, Meherpur

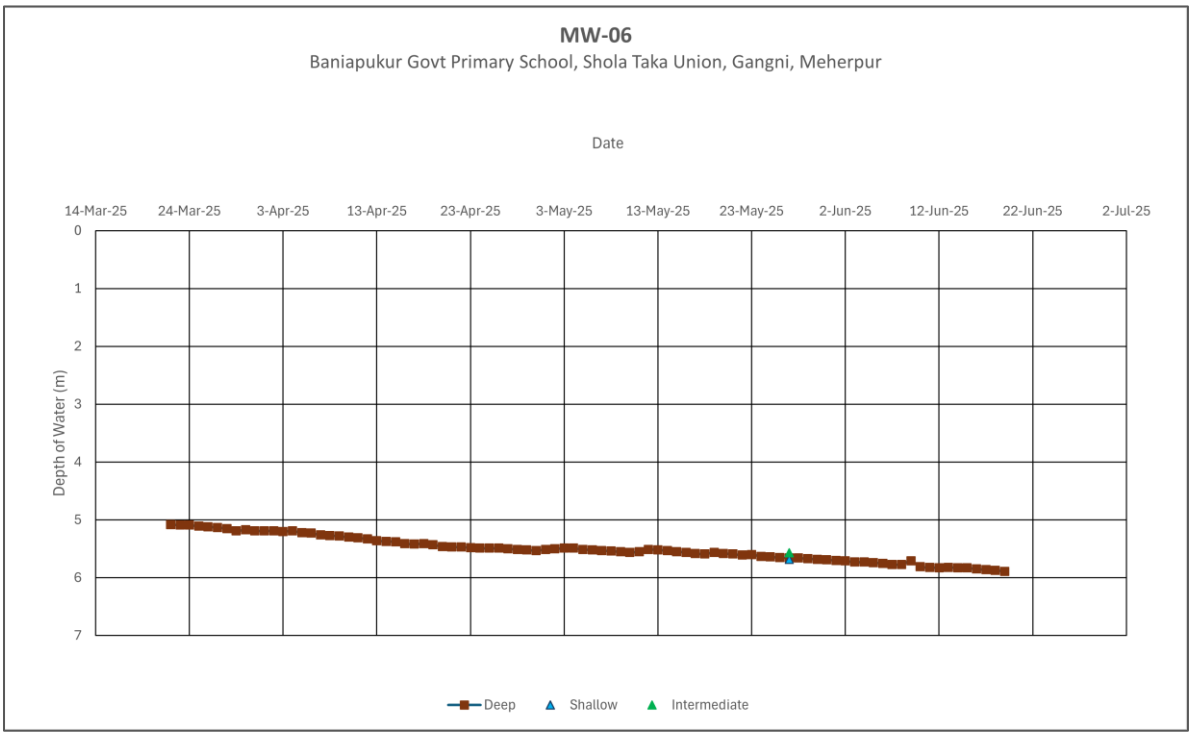

Figure 20: Ground Water Level in MW-06 Baniapukur Govt Primary School, Shola Taka Union, Gangni, Meherpur

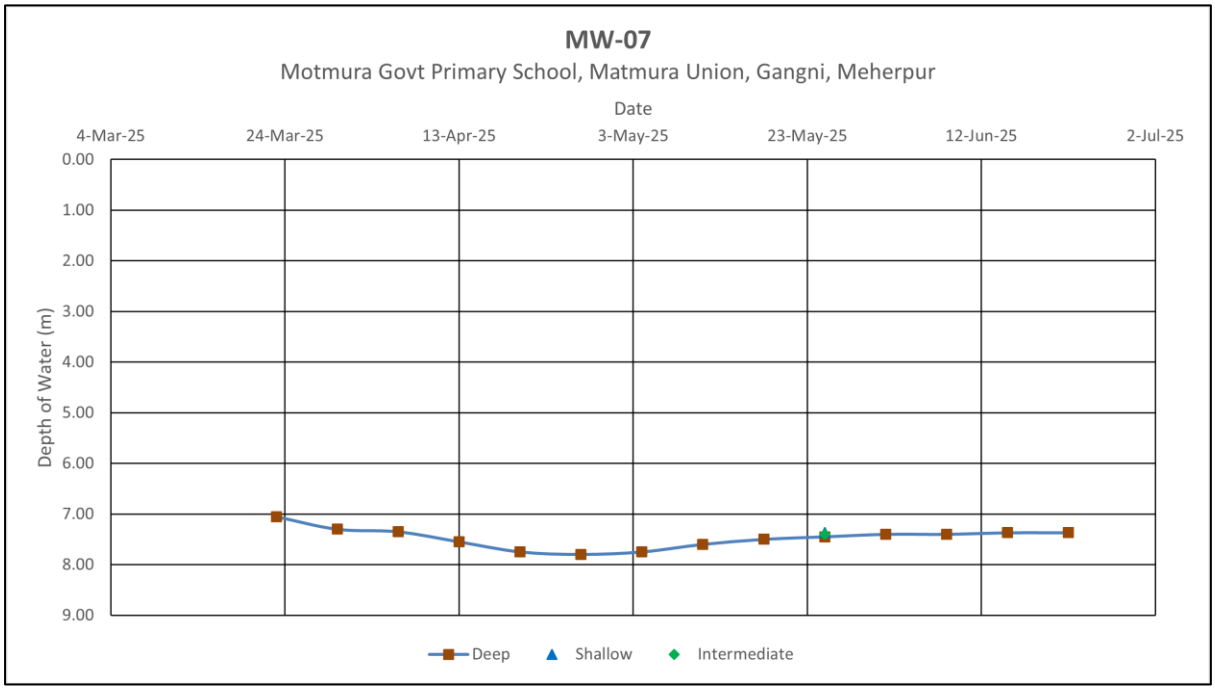

Figure 21: Ground Water Level in MW-07 Motmura Govt Primary School, Matmura Union, Gangni, Meherpur

Analysis of groundwater level data from monitoring wells MW-01, MW-02—located in Mujibnagar and MW-07- located the northern part of Gangni Upazila (Map 01)—indicates a general declining trend in water levels during the last of May. However, a noticeable rise in water levels toward the end of April is likely attributable to the onset of seasonal rainfall.

Given the geological setting of Meherpur District, it is plausible that minor fault zones or subsurface fractures exist within the study area. These features may serve as preferential pathways, facilitating localized recharge of the confined aquifer during periods of significant precipitation. Furthermore, if the confining layer is semi-permeable rather than strictly impermeable, vertical leakage from overlying unconfined or perched aquifers may occur. Such leakage, particularly during sustained rainfall events, can contribute to a delayed rise in groundwater levels within the confined system.

In contrast, monitoring wells MW-03, MW-04, MW-05, and MW-06—located in Meherpur Sadar and Gangni Upazila (Map 01)—exhibit a consistent decline in groundwater levels from March to June 2025, despite the occurrence of rainfall. This observation suggests that these wells may be hydraulically isolated from active recharge zones or are located in areas with limited vertical or lateral hydraulic connectivity to recharge sources.

5.1.2 Groundwater Level in Shallow and Intermediate Aquifer

Groundwater levels in the shallow and intermediate zones of the study area appear to correspond closely with those observed in the deep aquifer. However, as these measurements were collected using manual logging methods, data is available only for a single observation conducted at the end of May. Due to the limited temporal resolution of the dataset, no definitive interpretation or conclusions can be drawn regarding the hydrogeological behavior or interactions among the aquifer layers.

5.2 Water Quality Data

In January 2025, CGR initiated in-situ testing at 35 existing production wells located across 18 unions and 2 municipalities (paurashavas) prior to the commencement of drilling for the installation of monitoring wells. The field investigations included measurements of electrical conductivity (EC), total dissolved solids (TDS), pH, and arsenic concentrations, as well as slug tests and water sampling for subsequent ion analysis at a laboratory in Dhaka.

Upon completion of the drilling campaign, CGR conducted the same suite of in-situ tests at 21 newly constructed monitoring wells in Meherpur district. In total, 56 wells (map: 03) were investigated, categorized as follows:

Table 1: Number of Wells for Water Sampling and Field Test

Type of Well	Number of Wells
Shallow	29
Intermediate	20
Deep	7
Total Well	56

The preceding dry season report presented the analytical results of key physicochemical parameters, including electrical conductivity (EC), total dissolved solids (TDS), pH, and arsenic concentrations, obtained from both existing production wells and newly installed monitoring wells. A total of 56 groundwater samples were collected for comprehensive hydrochemical characterization. Major cations and trace elements targeted for analysis include sodium (Na^+), calcium (Ca^{2+}), magnesium (Mg^{2+}), potassium (K^+), iron (Fe), manganese (Mn), as well as key anions such as bicarbonate (HCO_3^-), chloride (Cl^-), sulfate (SO_4^{2-}), and nitrate (NO_3^-). These samples are currently undergoing detailed laboratory analysis at the Dhaka facility.

In addition, constant-rate slug tests were carried out by CGR to evaluate aquifer hydraulic properties, and grain size distribution analyses were conducted to estimate the hydraulic conductivity (K) of selected monitoring wells. The results of the ion and trace element analyses, along with the integrated interpretation of all hydrogeological parameters, will be incorporated into the forthcoming report titled *"Report on Groundwater Scenario of the Whole Hydrological Year along with Identification of Potential Area of Groundwater Recharge and Drawing, and Surface water and Groundwater Interfacing Model including GIS Shapefile and Thematic Map."*

6 Drought Analysis

Drought analysis is crucial for Bangladesh, as it is an agriculture-dependent country. Farmers across all districts cultivate crops throughout the year, relying primarily on groundwater, while in some areas, surface water from rivers and wetlands (bills) is extensively utilized. However, groundwater recharge and the availability of sufficient water in rivers and wetlands largely depend on rainfall, which plays a vital role in Bangladesh's hydrological cycle. Additionally, rainfall helps maintain soil moisture, which is essential for crop production. This report aims to assess the occurrence of rainfall using the Standardized Precipitation

Index (SPI) in the Meherpur district. It is obvious that Soil moisture, agricultural production, and hydrological conditions are all impacted by variations in the SPI. The following table highlights the importance and relevance of different SPI time scales for drought analysis.

Table 2: SPI and its relation to the impact on agriculture and water resources

SPI Scale	Duration (months)	Drought Type	Importance	Impact on Agriculture & Water Resources
SPI-1	1	Short-term	Detects sudden rainfall changes, key for immediate drought assessment.	Identifies quick drought stress in crops like rice; it affects short-term soil moisture.
SPI-3	3	Seasonal	Evaluates seasonal drought impact, crucial for crop growth assessment.	Impacts key agricultural seasons (Kharif, Rabi); influences soil moisture availability.
SPI-6	6	Medium-term	Assesses extended moisture availability; useful for irrigation planning.	Affects irrigation, especially in Kharif-2; long-term soil moisture deficit may develop.
SPI-12	12	Long-term	Monitors annual moisture trends, indicating climate shifts.	Captures prolonged droughts or excessive rainfall; affects groundwater recharge and overall agricultural productivity.

6.1 Methodology:

For the calculation of SPI, long-term precipitation data is required for a given area. Based on historical precipitation records, SPI quantifies precipitation deficits or surpluses relative to a long-term climatological baseline. Precipitation is often skewed than normal distribution which needs to be normalized Before calculating SPI for different time frames. This skewness occurs because most of the year is dominated by small amounts of rainfall, while extreme rainfall events are limited to fewer months. Precipitation data often does not follow a normal distribution. Therefore, this study utilized gamma distribution, a flexible statistical model that can accurately represent the wide range of precipitation amounts, including both dry and wet periods. This approach is used to transform precipitation data into a normal distribution through cumulative probability estimation. Additionally, months having zero rainfall are common in precipitation databases, which prevents the data from being normally

distributed. To address this, a mixed probability approach combining gamma and exponential distributions is applied, ensuring a more accurate and reliable SPI calculation. During this conversation process, historical precipitation data was fitted to a probability distribution, transforming it into a standardized normal distribution (Z-score), and categorizing drought severity based on SPI thresholds. For SPI-1, SPI-3, and SPI-6, the gamma distribution is commonly used due to its flexibility in modeling skewed precipitation data. By calculating SPI at four times, a comprehensive picture of drought dynamics and their cascading effects on vegetation conditions was captured. This enables a deeper understanding of short- and long-term impacts on ecosystems.

6.2 Study Area

This study focuses on Meherpur District, located in southwestern Bangladesh (23.8°N, 88.6°E), spanning 716 km^2 within the in active Ganges delta. The district experiences a tropical monsoon climate with an annual rainfall of approximately 1,500 mm, mostly occurring during the monsoon season (June–October). It also features a tropical wet and dry (savanna) climate, with an average temperature of 28.33°C, peaking at 39°C in April and dropping to 10.5°C in January which is 0.59% higher than Bangladesh's average (Rahman et al., 2023). Rainfall variability, influenced by the Indian monsoon and the El Niño-Southern Oscillation (ENSO), has contributed to frequent droughts (Mirza, 2003; Shahid, 2010)

Cropping seasons in Bangladesh are classified into Kharif- 1(March to June), Kharif 2 (July to October) and Rabi (November to February) where Meherpur district is not an exception but due to monsoon rainfall only the two season is significant in Bangladesh (Faridatul and Ahmed, 2020). Over 70% of rainfall occurs in monsoon season (Hossain et al., 2019), while annual rainfall of Meherpur District is the lowest of all Bangladesh approximately 1,500 mm (BMD,2022; Moniruzzaman et al., 2018) Meherpur's economy heavily relies on agriculture, with three key cropping seasons: Kharif-1, Kharif-2, and Rabi. Aman and Aus rice rely on seasonal rainfall, whereas Boro rice requires groundwater irrigation. The Standardized Precipitation Index (SPI) is a valuable tool for analyzing meteorological drought. However, this study adapts the SPI approach to assess agricultural drought specifically within the Meherpur District. Ultimately, this analysis will support the creation of climate-resilient agricultural strategies for the area

6.2.1 Data Collection

For this study, daily precipitation data were sourced from the Climate Hazards Group InfraRed Precipitation with Station (CHIRPS) dataset, which is widely recognized for its

ability to combine satellite-derived estimates with in-situ station data. CHIRPS provides high spatial resolution (~0.05°, approximately 5 km per pixel) and long-term temporal coverage, making it a reliable choice for monitoring precipitation variability and analyzing drought conditions (Funk et al., 2015). The data was extracted using Google Earth Engine for the period from January 1, 1990, to December 31, 2024. Precipitation values were collected for a single representative midpoint within Meherpur District, as the area is too small to exhibit significant variability at the CHIRPS resolution (~5 km per pixel). The dataset offers a long-term record essential for robust drought analysis, capturing both short-term (SPI-3) and medium-term (SPI-6) precipitation variability. The daily precipitation data for the selected location were stored in CSV format, including the date and the corresponding precipitation measurements in millimeters (mm). This approach ensures that the dataset provides a consistent and representative basis for analyzing drought patterns within the district.

6.2.2 Data Processing

The processing of precipitation data for the Standardized Precipitation Index (SPI) calculations involved a few steps that are given in the following section:

The first step in the data processing was to address missing daily precipitation values. This was accomplished by substituting the missing values with the average precipitation calculated from surrounding time periods which helps to maintain the continuity of the data series. To maintain the integrity of the SPI calculations, adjustments for zero and extreme negative rainfall values were made by replacing them with a small threshold ranging from 0.01 mm to 1 mm. This approach ensures that the calculations remain robust while addressing the limitations posed by zero or negative values in the dataset (WMO, 2012; McKee et al., 1993). Since the gamma distribution cannot accommodate zero values, any monthly totals that resulted in zero (after daily adjustments) were substituted with a minimal value of 1 mm. This substitution enables the complete dataset to be modeled without causing computational errors. The given table shows the aggregate of monthly precipitation data to be able to achieve the SPI values for a particular location:

Table 3: Monthly rainfall data aggregation to the corresponding SPI values

SPI	Monthly Rainfall Data
SPI-1	Use raw monthly precipitation totals.
SPI-3	Compute 3-month rolling sums (e.g., Jan–Mar, Feb–Apr).
SPI-6	Compute 6-month rolling sums (e.g., Jan–Jun, Feb–Jul).
SPI-12	Compute 12 months rolling sums (Jan-Dec)

6.2.3 Gamma Distribution Fitting

The collected data was modeled using a gamma distribution because rainfall measurements are always positive and typically exhibit a pattern of many low to moderate values with only a few extreme rainfall events. This type of data is "positively skewed," meaning it has a higher frequency of smaller rainfall events and fewer high-intensity events, which creates an asymmetric distribution. Monthly precipitation data often display this characteristic, making the gamma distribution an ideal choice for modeling such data. The gamma distribution is specifically designed for positive values and effectively captures the asymmetry of rainfall patterns. It is a mathematical model defined by two parameters: the shape parameter (α) and the scale parameter (β), which together describe the data's distribution. This model helps estimate the likelihood of varying rainfall amounts, accounting for frequent low rainfall and occasional heavy rainfall. Maximum Likelihood Estimation (MLE) was used to determine these parameters, ensuring the fitted gamma distribution closely aligns with the observed data. The probability density function (PDF) of the Gamma distribution is:

$$g(x) = \frac{\left[x^{(\alpha-1)} * e^{-\frac{x}{\beta}}\right]}{[\beta^{\alpha} * \Gamma(\alpha)]}, x > 0$$

Where , α is the shape parameter, β is the scale parameter and Γ(α) is the Gamma function.

All these parameters (i.e., calculate the alpha and beta value) were estimated using the MLE method in python environment.

6.2.4 SPI Calculation:

Once the gamma distribution was fitted to the precipitation data, the next step was to calculate the cumulative distribution function (CDF). The CDF transforms the modeled precipitation values into probabilities, providing a complete probabilistic description of the data. For example, it allows us to answer the question, “What is the probability of observing 50 mm of rain or less in a month?” Mathematically, the CDF is expressed as:

$$F(x) = \int_0^x g\ (t)dt$$

Rainfall varies from one place to another. To compare the weather conditions across different areas or time periods, we need a common scale. That’s where standard normal transformation comes in. The probabilities obtained from the CDF where then transformed into a standardized scale known as the Standardized Precipitation Index (SPI) where a value of 0 means the rainfall is exactly average. Positive values mean there is more rain than average.

Negative values mean there is less rain than average. The SPI value was derived by transforming the CDF to the standard normal distribution:

$$SPI = \Phi^{-1}\big(F(x)\big)$$

Where

(Φ^{-1}) is the inverse of the standard normal CDF.

This transformation standardizes the precipitation values, ensuring a mean of 0 and a standard deviation of 1: SPI > 0: Wet conditions and SPI < 0: Dry conditions. SPI values were classified into drought and wetness categories:

Table 4: Categories of drought scenarios based on SPI value range (McKee et al 1993)

Category	SPI value range
Extremely Dry	SPI < -2.0
Severely Dry	-2.0 ≤ SPI < -1.5
Moderately Dry	-1.5 ≤ SPI < -1.0
Near Normal	-1.0 ≤ SPI ≤ 1.0
Moderately Wet	1.0 < SPI ≤ 1.5
Very Wet	1.5 < SPI ≤ 2.0
Extremely Wet	SPI > 2.0

6.2.5 Mann-Kendall Trend Analysis

An important estimate was to detect trends in various cropping seasons using the SPI time series data in the given area, the non-parametric Mann-Kendall (MK) test was employed. The test is widely used for hydroclimatic time series analysis as it is robust to non-normal distributions and missing data (Mann, 1945; Kendall, 1975). The test assesses the presence of a monotonic increasing or decreasing trend in the time series by evaluating the ranks of data points. Seasonal Mann-Kendall Test To examine seasonal trends in SPI values, the Seasonal Mann-Kendall (SMK) test was applied using the pymannkendall Python package. The test accounts for periodicity in time series data and is particularly suitable for detecting trends in climatic datasets.

For each SPI timescale (i.e., SPI-1, SPI-3, SPI-6, and SPI-12), the seasonal Mann-Kendall test was performed separately for each cropping season (*Kharif*, *Kharif 2*, and *Rabi*). The test was conducted with a periodicity of 12 months, assuming a monthly resolution in the dataset. The trend analysis provided key statistical outputs, including: (1) Trend direction

(increasing/decreasing/no trend, (2) Significance level (p-value), (3) Kendall's Tau correlation coefficient and (4) Slope of the trend line (Sen's slope estimator).

p -value <0.05. and Z score > -2.00 is acceptable to identify the trend analysis.

$$S = \sum_{i-1}^{n-1} \sum_{j-i+1}^{n} sgn(xj - xi)$$

Where

$$sgn(xj - xi) = \begin{cases} +1, & if\,(xj - xi) > 0 \\ 0, & if\,(xj - xi) = 0 \\ -1, & if\,(xj - xi) < 0 \end{cases}$$

For large sample sizes, the variance of S is given by:

$$Var(S) = n(n-1)\,(2n+5)/18$$

In the presence of ties, the variance is adjusted as follows:

$$Var(S) = n(n+1)\,(2n+5) - \sum_{i-1}^{m} ti(ti-1)(2ti+5)\,/18$$

The standardized test statistic Z is computed to assess significance:

$$Z = \begin{cases} \dfrac{s-1}{\sqrt{var(S)}}, & if\ S > 0 \\ 0, & if\ S = 0 \\ \dfrac{s+1}{\sqrt{var(S)}}, & if\ S < 0 \end{cases}$$

Furthermore, Sen's slope estimator was used to quantify the magnitude of the trend:

$$\beta = median\,((xj - xi)/(j - i))\ for\ all\ i < j$$

6.3 Results

6.3.1 Rainfall

Meherpur district experiences an average of ~ 1500mm rainfall having varying patterns of precipitation which is evident from the rainfall data from 1990 to 2024.

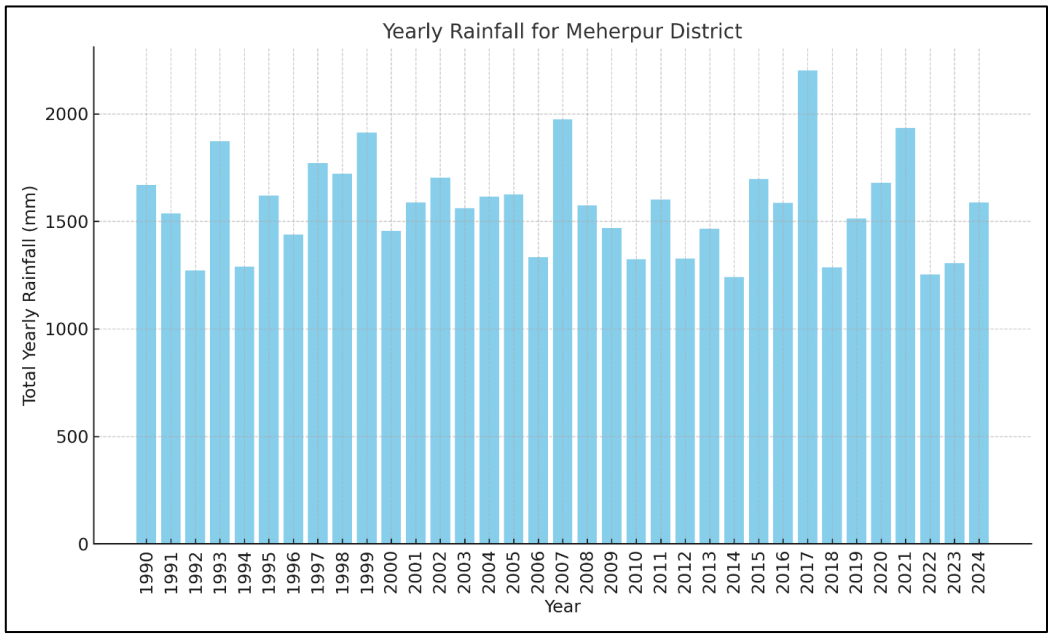

Figure 22: Yearly Rainfall Distribution across 24 years in Meherpur District

Figure 1 showing total of the thirty-four years rainfall data, the years: 1992, 2006, 2014, 2018, and 2022 recorded the lowest rainfall, approximately 1241 mm, while the years 2017, 2021, and 2007 experienced the highest rainfall, exceeding 1750 mm. A noticeable declining trend in rainfall started from 2008, with significant fluctuations observed in subsequent years. On average, the yearly rainfall is around 1500 mm. Below is the summary of the total 34 years of average monthly rainfall along with skewness values.

Table 5: Monthly rainfall statistics, including the mean rainfall (in millimeters) and the skewness of the rainfall distribution for each month

Month	Mean Rainfall(mm)	skewness
1	1.08432631	1.45310818
2	7.28379963	1.116424903
3	29.76132576	2.090342354
4	58.8076144	0.427428969
5	155.0488638	0.810444853
6	237.7901331	0.115503725
7	319.4634169	0.282430382
8	268.8162599	0.674055387
9	237.0139994	0.694023242
10	145.3770728	1.312331908
11	10.70866934	1.386555993
12	0.790683044	2.746839204

Variation in mean rainfall and the nature of rainfall distribution across the months is quite evident in the study area. Table 3 shows the seasonal patterns, while skewness provides insights into the probability of extreme rainfall events. Together, these metrics are valuable for understanding water availability, drought risk, and flood potential in the region. A seasonal trend has been identified from the mean rainfall that varies significantly across the year. Highest mean rainfall was observed Months 6, 7, 8, and 9, indicating a monsoon season during these months. In contrast, Months 1 and 12 experienced the lowest means of rainfall, pointing to drier periods. Skewness measures the asymmetry of the rainfall distribution, helping to understand the likelihood of extreme rainfall events. Positive skewness **(Months 1, 2, 3, 5, 8, 9, 10, 11, 12)** indicates that the rainfall distribution has a longer tail on the higher side. In these months, most rainfall events are likely to be low to moderate, but there is a higher probability of occasional heavy rainfall events that can significantly increase the average. For example, Month 12 has the highest skewness value (2.75), suggesting the potential for rare but very heavy rainfall events during this month. Whilst the **Near-Symmetrical Skewness in** Months **(4, 6, 7)** with skewness values closer to zero have more symmetrical rainfall distributions, meaning rainfall is evenly distributed around the mean. Extreme low or high rainfall events are less likely. Among all months, Month 6 has the lowest skewness value (0.12), making it the closest to a symmetrical distribution. In a nutshell, the skewness values indicate a positive skew in most months, particularly in October, November, December, January, and March, where the significantly high skewness suggests that rainfall events are concentrated in the latter part of the year

6.3.2 Gamma Distribution:

To analyze drought patterns and precipitation distribution more effectively, a gamma distribution model was applied to the Standardized Precipitation Index (SPI) at timescales of SPI-1, SPI-3, SPI-6, and SPI-12. The table presents the gamma distribution parameters (shape and scale) for these timescales across different months, providing valuable insights into drought characteristics.

Table 6: Results of Gamma Distribution Parameters for SPI Drought Analysis

Month	SPI-1		SPI -3		SPI-6	
	Shape	Scale	Shape	Scale	Shape	Scale
1	3.563276	3.516307	6.366044	10.5431	36.31542	14.21522
2	3.430738	4.994671	7.123202	16.02971	26.60627	31.5894

3	2.913535	12.85477	19.57755	12.70493	35.97769	30.46064
4	3.082048	19.33604	25.27541	17.76881	41.41651	31.96962
5	9.126101	16.62091	22.76471	31.90435	44.57659	32.02054
6	13.3429	17.82486	26.20896	32.32375	37.24379	34.66324
7	7.496413	44.92465	26.0854	33.54198	29.64646	35.6014
8	9.976775	27.31975	19.63939	35.69732	21.23079	34.07165
9	9.691218	27.40825	11.58389	38.31342	14.11542	33.27374
10	3.445375	47.27823	4.139626	43.60282	9.28546	26.37803
11	0.93128	16.43741	2.668735	11.48119	9.433642	15.29013
12	1.430177	1.608414	5.348664	5.942688	23.94515	11.66952

The gamma distribution parameters reveal varying drought characteristics across different SPI timescales. For SPI-1 (monthly), the shape parameter (0.93–13.34) and scale parameter (1.6–47.28) indicate fluctuating short-term severity, with fewer extreme drought events over time and broader precipitation distributions in some months. SPI-3 (3-month) shows greater variability, with shape (4.99–44.92) and scale (10.54–43.60) parameters highlighting more pronounced and prolonged droughts. SPI-6 (6-month) exhibits significant variability, with shape values (9.29–44.58) and high scale values (11.67–35.60) reflecting severe, prolonged droughts, especially mid-year. SPI-12 (12-month) parameters show the widest range, with shape (31.58–49.29) and scale (21.60–73.67) values indicating the most extended and severe drought conditions.

6.3.3 SPI Timeseries Analysis

Monitoring wet and dry cycles, identifying long-term drought patterns, and evaluating the start, length, and recovery of droughts over a variety of periods are all made possible by time series analysis of the SPI index. It helps with successful drought resilience and adaptation methods by offering a standardized, geographically similar metric for early warning, managing water resources, and comprehending climate variability. One useful tool for a general evaluation of dry and wet conditions is the SPI trend over rainfall data, which allows for a rapid assessment of rainfall. When rainfall and SPI graphs are combined, important

information about rainfall variability and the distinction between wet and dry periods can be obtained. The relationship between precipitation trends and standardized anomalies can be better understood by combining rainfall data with all SPI indices in a single graph, as demonstrated in (Figure 2). This provides a better understanding of departures from historical averages.

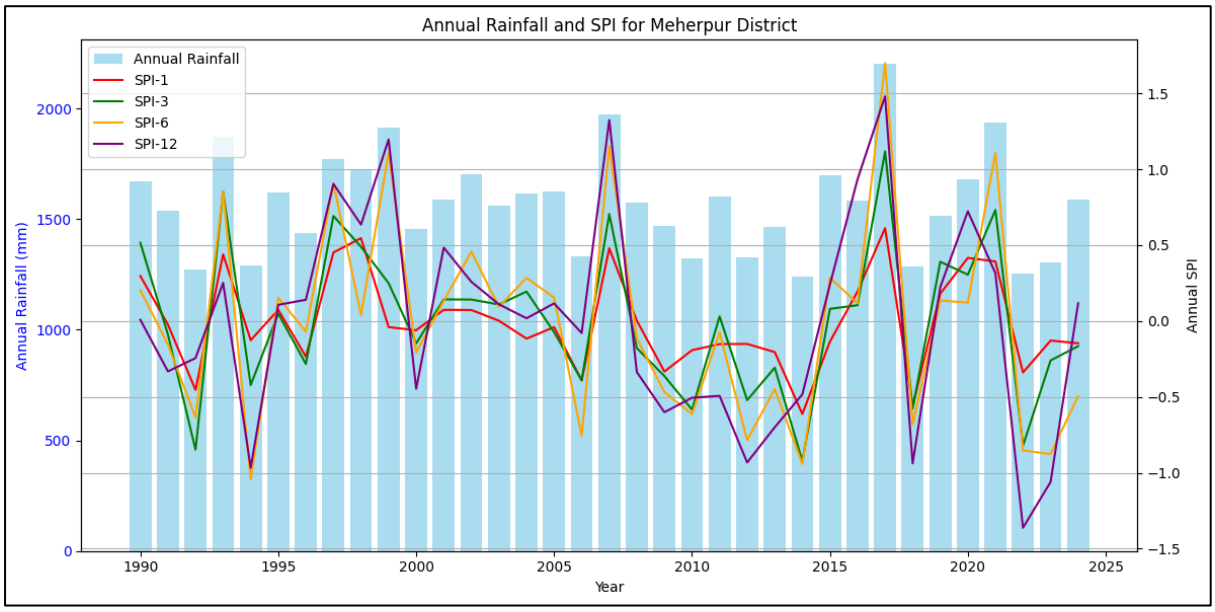

Figure 23: Annual Rainfall and SPI values are shown for Meherpur District

In the case of the rainfall data, significant peaks are observed in the years high rainfall years (1999, 2007, 2017 and 2021) while noticeable dips occur in lowest rainfall years (2006 ,2014 ,2018, 2021 and 2022). These anomalies provide an intuitive way of seeing how rainfall varies on a yearly basis. When overlaying the SPI indices, a clear correlation emerges, as the SPI values tend to rise during high-rainfall years and fall during years with lowest rainfall years. In 2017 SPI 6 showed the wettest condition of Meherpur District. SPI-12 showing lowest drops in 2022 and 2023 showing drought conditions. From 2005 to 2015 showing a tendency of negative value for all the SPI Indices.

Interestingly, longer-term SPIs, such as SPI-6 and SPI-12, display more stable and smoothed trends. These indices are cumulative in nature, which makes them less responsive to the immediate, short-term fluctuations in annual rainfall.

In the second instance, a time series plot showcasing four different SPI time scales (SPI-1, SPI-3, SPI-6, and SPI-12) for the Meherpur district reveals how SPI variability differs over time. As illustrated in Figure 3, these four indices provide a comprehensive view of precipitation trends, ranging from short-term fluctuations (SPI-1) to extended long-term changes (SPI-12). (Figure 3)

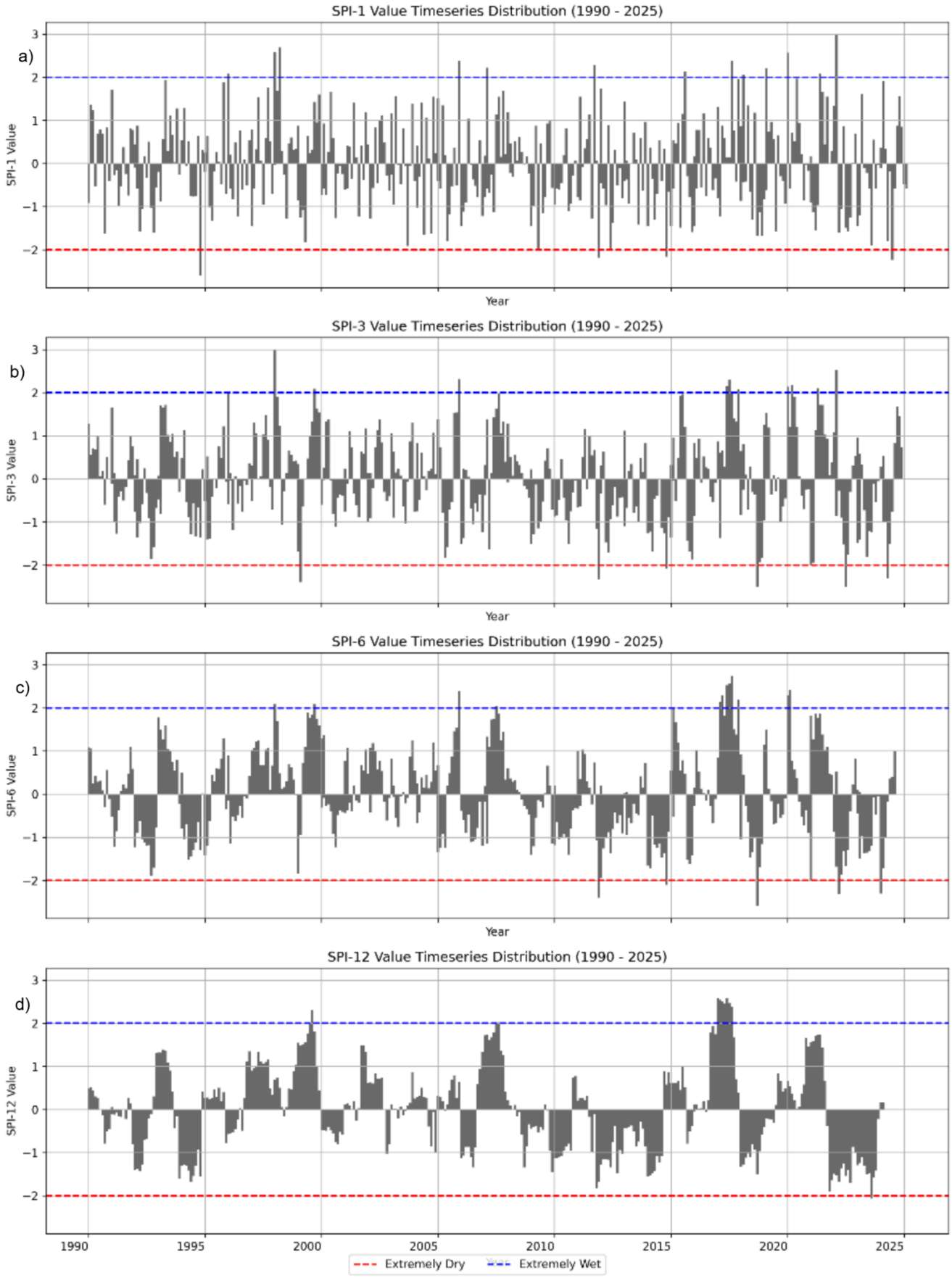

Figure 24: SPI Timeseries Distribution from 1990 to 2025

These plots (a,b,c,d) in **Figure 24** provide an insightful analysis of how precipitation trends fluctuate across 1990 to 2025 for four different time scales: a)SPI-1 (short-term), b)SPI-3 (seasonal),c) SPI-6 (extended), and d) SPI-12 (long-term). Figure 3 illustrates the plots and a breif interpretation of these plots are given below

a) SPI-1 Value Timeseries Distribution (1990 - 2025): This subplot reflects short-term drought conditions, showing significant variability in precipitation patterns. Notable drought events include September 1994, where the SPI-1 value dropped to -2.698 indicating extreme dryness and also in 2014. Other severe droughts occurred in October 2011 and June 2024, with SPI-1 values reaching -2.187 and -2.236, respectively 2012 also showing drought conditions with noticable negetive value.

b) SPI-3 Value Timeseries Distribution (1990 - 2025): The SPI-3 value, representing seasonal drought conditions, provides a broader view of precipitation deficits. Key drought periods are observed in 1994, 1999, 2018, and 2022, with extreme dryness recorded during these years. From 2005 to 2015 and in the 2020s, multiple months with negative SPI-3 values signal an increase in seasonal drought intensity. This trend indicates a worsening drought pattern over time, affecting crop yields and water resources.

c) SPI-6 Value Timeseries Distribution (1990 - 2025): SPI-6, which represents 6-month precipitation anomalies, effectively highlights extended drought periods. Notable drought events, such as those in April 1994, July 2012, and October 2018, are evident, with SPI values dropping below -2, indicating prolonged dry spells. More recently, drought conditions were also observed in 2022 and 2024. The period from the 2010s to the 2020s exhibits a marked increase in the frequency of negative SPI-6 months, except for the wetter years of 2017 and 2020, underscoring its significance for assessing long-term drought trends

d) SPI-12 Value Timeseries Distribution (1990 - 2025): The SPI-12 index highlights long-term droughts, which were most severe during the early 1990s, 2008-2014, and 2018. More recent years, particularly 2022-2024, show a dominance of moderately dry periods, with SPI values frequently dipping below -1. Major long-term droughts, such as in September 2011 and 2022 years showing nearly -1.90 SPI value which is visible in the graph and June 2024, show SPI values dropping below -2, signaling severe water scarcity over extended periods. This shift towards drier conditions poses significant risks to agriculture, especially over multiple cropping seasons.

6.3.4 Drought Category:

A uniform approach to assessing droughts' impacts on ecosystems, agriculture, and water resources, as well as guiding risk management decisions, is provided by drought categories. A nation that depends heavily on agriculture, such as Bangladesh, needs detailed information on droughts to support early warning, historical comparisons, and effective communication with the public and policymakers (Wilhite, D.A et al 2014). By classifying the severity of drought, these categories enable timely actions and long-term planning for climate resilience (Krishna Prabhakar 2022) Several observations were taken into consideration for this study, including the percentage of drought categories across the full dataset and the proportion of drought categories monthly. Additionally, the drought length was assessed in relation to Bangladesh's three primary cropping seasons in addition with the average SPI for the three cropping seasons was also computed. The next section provides a brief description of each of these assessments.

The SPI was used to calculate the percentage distribution of the various drought, near normal, and wetness categories in Meherpur district over a range of time periods (Figure 4). It is clear from the assessment that "Near Normal" events predominate in the study area, with percentages above 60% across all SPI time ranges. Conversely, the percentages of extreme categories such as "*Extremely Dry*" and "*Extremely Wet*" are far smaller. In contrast to SPI-6 and SPI-12, which place more emphasis on more stable conditions, the SPI-1 and SPI-3-time scales show somewhat greater variability in drought and wetness categories.

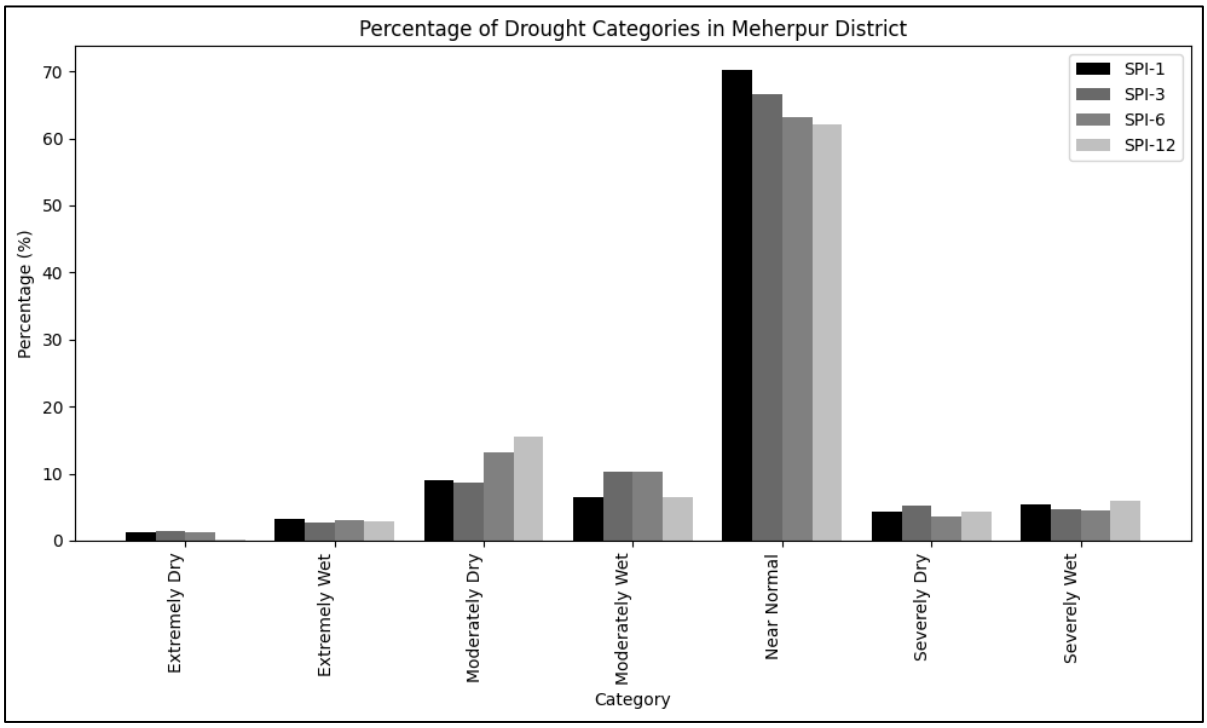

Figure 25: Drought category percentage in Meherpur District from 1990 to 2024

6.3.4.1 Monthly Drought Categories

The distribution of drought categories across all the months is shown below:

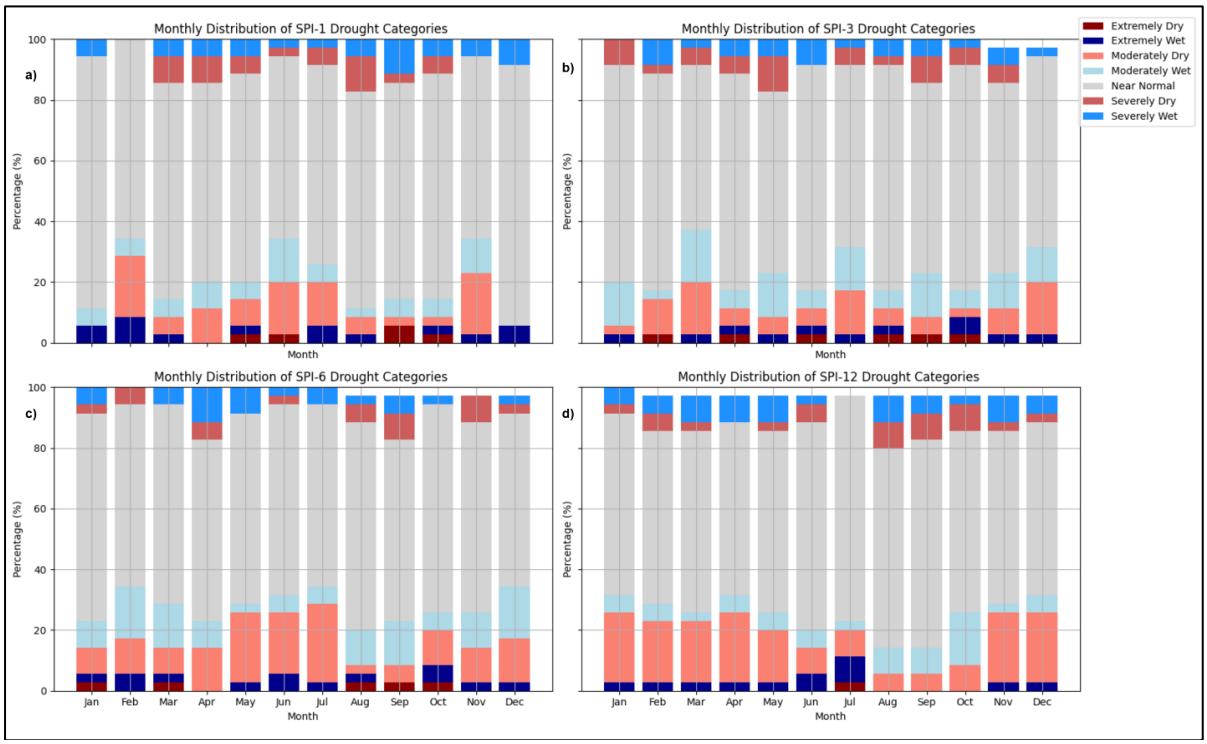

Figure 26: Monthly Drought Categories Percentage in Meherpur District from 1990 to 2025

As shown in Figure 5, "Near Normal" conditions prevail for at least 60% of the time across all months. In contrast, "Severely Dry" and "Moderately Dry" conditions are predominantly observed from March to August, with a probability of around 10%, particularly for SPI-1 and

SPI 6. SPI-12, however, shows a higher percentage of "Moderately Dry" conditions above 15 % from February to June, highlighting the extended duration of moderate drought during this period. These months exhibit higher rates of moderate to severe drought across all SPI periods, indicating increased vulnerability to drought during this time. Despite these fluctuations, near normal conditions (represented by gray bars) dominate throughout the year, suggesting that deviations from historical averages are not extreme in most months.

6.3.4.2 Seasonal Drought Characteristics:

Figure 6 illustrates the seasonal drought characteristics based on the three cropping seasons in the study area. In the Kharif season, SPI values reflect an increasing drought duration, ranging from approximately 1 month for SPI-1 to about 3.5 months for SPI-12. This suggests a greater accumulation of drought over the long term. In contrast, Kharif 2 exhibits relatively shorter drought durations, typically staying below 2 months across most SPI periods. However, the Rabi season demonstrates a significant increase in drought duration, particularly for SPI-12, which extends to about 4.5 months in the Meherpur District, indicating a prolonged dry phase.

Across all cropping seasons, SPI-1 shows a relatively consistent drought duration, highlighting the short-term nature of the drought during this period. On the other hand, SPI-6 and SPI-12 exhibit more fluctuations in drought duration, with SPI-6 showing slightly longer drought periods compared to SPI-12 during the Kharif 2 season. This reflects the varying sensitivity of the SPI indices to short-term and long-term changes in precipitation patterns, offering a nuanced view of seasonal drought dynamics.

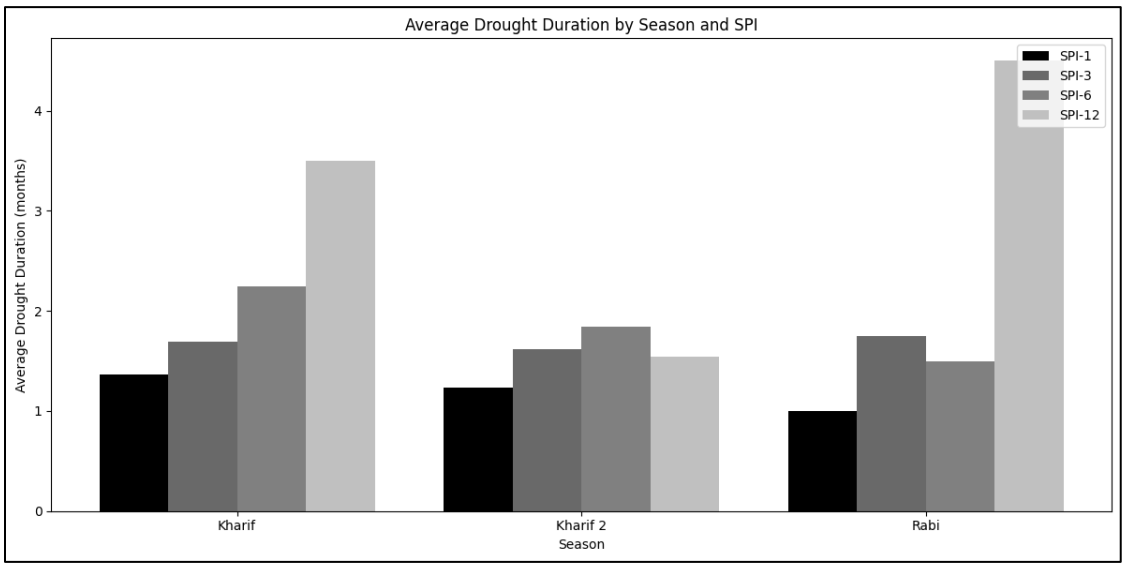

Figure 27: Seasonal average Drought duration months in Meherpur District

6.3.4.3 Average SPIs in Cropping Season:

Figure 7 displays the average SPI values for SPI 1, SPI 3, SPI 6, and SPI 12, which show a fluctuation in drought conditions from 2014 to 2025. For SPI 1 average SPI shows a moderate value within near normal value -1 to 1 SPI value across all seasons. The average SPI 1 displays a moderate value (i.e., between -1 and 1) that is close to normal SPI values for all seasons. However, SPI 3 exhibits seasonal variations, with Kharif 2 seeing a sharp decline in SPI value that crosses the moderately dry SPI value of -1. According to SPI 6, the Rabi season has been declining from 2020 to 2024.SPI 12 shows that every month's SPI value is rising and falling from year to year, such as from 2014 to 2017, when it increased, then fell for a year in 2018, before rising once more in the most recent years, indicating that the drought conditions have gotten worse recently.

Figure 28: Seasonal Average SPI values in Meherpur District

6.3.5 Trend Analysis:

Mann Kendall Trend was used for the trend analysis in this study. The seasonal Mann-Kendall trend analysis revealed that there were no statistically significant trends in short-term drought indicators across the Kharif, Kharif 2, and Rabi seasons. In contrast, medium- and long-term drought indicators exhibited significant decreasing trends. Notably, the 6-month SPI during the Kharif 2 season showed a significant decreasing trend, and the 12-month SPI during the Kharif season also exhibited a significant decline. These findings suggest a shift

towards drier conditions during these critical growing periods, which may increase the risk of drought.

Table 7: Mann Kendall trend statistics on three cropping seasons of the study area

Test	Trend	Significant	p-value	z-score	Kendall's Tau	Slope	Intercept
SPI-1Kharif	no trend	FALSE	0.727	-0.35	-0.0241	-0.017	0.1772
SPI-1Kharif 2	no trend	FALSE	0.446	-0.761	-0.0508	-0.018	0.0955
SPI-1Rabi	no trend	FALSE	0.097	-1.658	-0.1056	-0.005	-0.2594
SPI-3Kharif	no trend	FALSE	0.696	-0.391	-0.0267	-0.01	0.215
SPI-3Kharif 2	no trend	FALSE	0.104	-1.626	-0.1079	-0.047	0.215
SPI-3Rabi	no trend	FALSE	0.437	-0.777	-0.0523	-0.011	0.1903
SPI-6Kharif	no trend	FALSE	0.225	-1.214	-0.108	-0.031	0.1055
SPI-6Kharif 2	decreasing	TRUE	0.03	-2.166	-0.1441	-0.065	0.2792
SPI-6Rabi	no trend	FALSE	0.753	-0.315	-0.022	-0.011	0.0711
SPI-12Kharif	decreasing	TRUE	0.001	-2.039	-0.1364	-0.055	0.2963
SPI-12Kharif 2	no trend	FALSE	0.15	-1.438	-0.0966	-0.055	0.2963
SPI-12Rabi	no trend	FALSE	0.075	-1.784	-0.1189	-0.054	0.3897

7 Discussion

The initial phase of this hydrogeological investigation successfully established a foundational monitoring network across Meherpur District, covering three upazilas and seven strategically selected sites. A total of 21 monitoring wells—comprising shallow (~100 ft), intermediate (~300 ft), and deep (~500 ± 100 ft) wells at each location—were installed to assess vertical and lateral variations in groundwater levels and quality.

Wet-season groundwater level data, collected between 22 March and 19 June 2025, serve as a critical baseline for evaluating aquifer conditions in the absence of significant recharge. Preliminary findings reveal both spatial and vertical variability in deep-well water level responses across the network. Several deep wells exhibited a gradual decline in groundwater levels throughout the pre-monsoon period, consistent with drawdown in confined and semi-confined aquifers. However, isolated cases of water level recovery observed in late April suggest localized recharge events, probably influenced by structural features such as minor faults or semi-permeable confining layers.

Groundwater samples collected for laboratory analysis of major and trace ions (Na^{+}, Ca^{2+}, Mg^{2+}, K^{+}, Fe, Mn, HCO_3^{-}, Cl^{-}, SO_4^{2-}, and NO_3^{-}) are expected to provide further insights into groundwater chemistry and possible geogenic or anthropogenic influences. Concurrently, CGR conducted constant-rate slug tests and grain size distribution analyses to evaluate aquifer hydraulic properties such as permeability and hydraulic conductivity—critical parameters for groundwater flow modeling and sustainable resource management.

A drought analysis of Meherpur Zilla was also conducted using the Standardized Precipitation Index (SPI) at four-time scales (SPI-1, -3, -6, and -12), based on CHIRPS rainfall data from 1990 to 2024. The results indicate an increasing trend of drought, particularly in SPI-6 and SPI-12 during the Kharif-2 and Rabi seasons, with rainfall variability significantly impacting groundwater recharge and agricultural productivity.

As this report focuses exclusively on wet-season data, it provides a vital reference point for understanding seasonal groundwater dynamics. Once the full year of monitoring is completed, integrating both wet- and dry-season data will enable a comprehensive assessment of recharge mechanisms, aquifer connectivity, and long-term groundwater sustainability in the region.

Continued monitoring, supported by laboratory results and aquifer property assessments, will enhance the capacity to develop targeted groundwater management strategies and inform broader development planning initiatives for Meherpur Zilla.

8 References:

1. Moniruzzam, M., Roy, A., Bhatt, C. M., Gupta, A., An, N. T. T., and Hassan, M. R.: Impact Analysis of Urbanization on Land Use Land Cover Change For Khulna City, Bangladesh Using Temporal Landsat Imagery, Int. Arch. Photogramm. Remote Sens. Spatial Inf. Sci., xlii-5, 757–760, https://doi.org/10.5194/isprs-archives-xlii-5-757-2018, 2018.
2. Rahman, M.S., Reza, A.H.M.S., Siddique, M.A.B. et al. Accumulation of arsenic and other metals in soil and human consumable foods of Meherpur district, southwestern Bangladesh, and associated health risk assessment. Environ Sci Eur 35, 47 (2023). https://doi.org/10.1186/s12302-023-00751-2
3. Hossain, M. S., Qian, L., Arshad, M., Shahid, S., Fahad, S., & Akhter, J. (2018). Climate change and crop farming in Bangladesh: an analysis of economic impacts. International Journal of Climate Change Strategies and Management, 11(3), 424-440.
4. Faridatul, M. I., & Ahmed, B. (2020). Assessing Agricultural Vulnerability to Drought in a Heterogeneous Environment: A Remote Sensing-Based Approach. Remote Sensing, 12(20), 3363. https://doi.org/10.3390/rs12203363
5. Shahid, S. (2010). Recent trends in the climate of Bangladesh. Climate Research, 42(3), 185–193. doi:10.3354/cr00889
6. Mirza, M. M. Q. (2003). Climate change and extreme weather events: can developing countries adapt? Climate Policy, 3(3), 233–248. doi:10.3763/cpol.2003.0330
7. Krishna Prabhakar, S.V.R., 2022. Implications of regional droughts and transboundary drought risks on drought monitoring and early warning: a review. Climate, 10(9), p.124.
8. Wilhite, D. A., Sivakumar, M. V., & Pulwarty, R. (2014). Managing drought risk in a changing climate: The role of national drought policy. *Weather and climate extremes*, *3*, 4-13.
9. McKee, T. B., Doesken, N. J., & Kleist, J. (1993, January). The relationship of drought frequency and duration to time scales. In Proceedings of the 8th Conference on Applied Climatology (Vol. 17, No. 22, pp. 179-183).

9 APPENDICES

9.1 APPENDIX: Table A-1: Location of Monitoring Well

Table A- 1: Location of the monitoring wells

MW No	Lat	Lng	Location	Well Type	Well Depth (ft)
MW-01S	23.668364	88.618485	Vobanipur Primary School, Monakhali Union, Mujib Nagar, Meherpur	Shallow	100
MW-01I	23.668334	88.618482		Inter	300
MW-01D	23.668061	88.618192		Deep	500
MW-02S	23.620756	88.606538	Anandabas Dakkhin Para Govt Primary School, Bagoan Union, Mujib Nagar, Meherpur	shallow	100
MW-02I	23.620741	88.606556		Inter	360
MW-02D	23.62092	88.605994		Deep	440
MW-03S	23.815158	88.626328	Ujalpur High School, Kutubpur Union, Meherpur Sadar, Meherpur	Shallow	100
MW-03I	23.815375	88.625838		Inter	300
MW-03D	23.815355	88.625874		Deep	390
MW-04S	23.722884	88.733103	Mominpur Govt Primary School, Pirojpur Union, Meherpur Sadar, Meherpur	shallow	100
MW-04I	23.722921	88.733171		Inter	300
MW-04D	23.723005	88.733194		Deep	500
MW-05S	23.810819	88.731965	Bashbaria Govt Primary School, Gangni Paurashava, Gangni, Meherpur	Shallow	100
MW-05I	23.810833	88.732028		Inter	300
MW-05D	23.810757	88.732004		Deep	455
MW-06S	23.835566	88.794543	Baniapukur Govt Primary School, Shola Taka Union, Gangni, Meherpur	Shallow	100
MW-06I	23.835622	88.794527		Inter	300
MW-06D	23.835708	88.794572		Deep	390
MW-07S	23.898399	88.834788	Motmura Govt Primary School, Matmura Union, Gangni, Meherpur	shallow	100
MW-07I	23.898398	88.834843		Inter	280
MW-07D	23.898397	88.834794		Deep	380

9.2 APPENDIX: Table A-2: Location of VES

Table A- 2: Location of VES

SlNo	lat	lng	Location Name	Upazila
ERT-01	23.709192	88.610437	Dariapur Playground, Dariapur, Mujibnagar	Mujib Nagar
ERT-02	23.632328	88.608547	Anandabash Playground behind Anandabash Girls High School, Bagoan, Mujibnagar	Mujib Nagar
ERT-03	23.679925	88.67875	Komorpur Secondary School, Mahajanpur, Mujibnagar	Mujib Nagar
ERT-04	23.77993	88.57395	Bajitpur Govt Primary School, Buripota, Meherpur Sadar	Meherpur Sadar
ERT-05	23.839616	88.612999	Tergharia Govt Primary School, Kutubpur, Meherpur Sadar	Meherpur Sadar
ERT-06	23.825234	88.68274	Shyampur Govt Primary School, Amjhupi, Meherpur Sadar	Gangni
ERT-07	23.746032	88.686194	Amjhupi Govt Health Complex Field, Amjhupi, Meherpur Sadar	Meherpur Sadar
ERT-08	23.715255	88.77673	Near Majhpara Sporting Club, Notun Dorbeshpur, Pirojpur Union, Meherpur Sadar	Meherpur Sadar
ERT-09	23.833839	88.75836	Opposite of CFM Secondary School, Gangni Paurashava, Gangni	Gangni
ERT-10	23.781947	88.740598	Near Nittyannandopur Playground, Dhankhola Union, Gangni	Gangni
ERT-11	23.784475	88.804593	Sanghat Chandamari High Schoo, Dhankhola Union, Gangnil	Gangni
ERT-12	23.850144	88.83589	Mikushis High School, Shola Taka Union, Gangni	Gangni
ERT-13	23.905773	88.815053	Near Motmura Eidgaon field, Matmura, Gangni	Gangni
ERT-14	23.936034	88.768265	Shahebnagar Govt Primary School, Kazipur Union, Gangni	Gangni
ERT-15	23.89041	88.720635	Near Tetulbaria Dayer Para Govt Primary Schoo, Tetulbaria Union, Gangni	Gangni